# Strong coupling from the revised ALEPH data for hadronic $\tau$ decays

Diogo Boito,[1] Maarten Golterman,[2] Kim Maltman,[3,4] James Osborne,[5] and Santiago Peris[6]

[1]*Physik Department T31, Technische Universität München, James-Franck-Straße 1, D-85748 Garching, Germany*

[2]*Department of Physics and Astronomy, San Francisco State University, San Francisco, California 94132, USA*

[3]*Department of Mathematics and Statistics, York University, Toronto, Ontario M3J 1P3, Canada*

[4]*CSSM, University of Adelaide, Adelaide, South Australia 5005, Australia*

[5]*Physics Department, University of Wisconsin–Madison, 1150 University Avenue, Madison, Wisconsin 53706, USA*

[6]*Department of Physics, Universitat Autònoma de Barcelona, E-08193 Bellaterra, Barcelona, Spain*

(Received 21 October 2014; published 3 February 2015)

We apply an analysis method previously developed for the extraction of the strong coupling from the OPAL data to the recently revised ALEPH data for nonstrange hadronic $\tau$ decays. Our analysis yields the values $\alpha_s(m_\tau^2) = 0.296 \pm 0.010$ using fixed-order perturbation theory, and $\alpha_s(m_\tau^2) = 0.310 \pm 0.014$ using contour-improved perturbation theory. Averaging these values with our previously obtained values from the OPAL data, we find $\alpha_s(m_\tau^2) = 0.303 \pm 0.009$ and $\alpha_s(m_\tau^2) = 0.319 \pm 0.012$, respectively. We present a critique of the analysis method employed previously, for example in analyses by the ALEPH and OPAL collaborations, and compare it with our own approach. Our conclusion is that nonperturbative effects limit the accuracy with which the strong coupling, an inherently perturbative quantity, can be extracted at energies as low as the $\tau$ mass. Our results further indicate that systematic errors on the determination of the strong coupling from analyses of hadronic $\tau$-decay data have been underestimated in much of the existing literature.

DOI: 10.1103/PhysRevD.91.034003 PACS numbers: 12.38.-t

## I. INTRODUCTION

Recently, Ref. [1], for the ALEPH collaboration, updated and revised previous ALEPH results for the nonstrange vector ($V$) and axial vector ($A$) spectral distributions obtained from measurements of hadronic $\tau$ decays. In particular, Ref. [1] corrects a problem in the publicly posted 2005 and 2008 versions of the correlations between different energy bins uncovered in Ref. [2].[1] The corrected data supersede those originally published by the ALEPH Collaboration [3,4].

One of the hadronic quantities of interest that can be extracted from these data is the strong coupling $\alpha_s(m_\tau^2)$ at the $\tau$ mass, through the use of finite-energy sum rules (FESRs) [5], as advocated long ago [6,7]. Both the ALEPH and OPAL [8] collaborations have done so by applying an analysis strategy, developed in Refs. [7,9], in which small, but non-negligible nonperturbative effects were estimated using a truncated form of the operator product expansion (OPE). A feature of the particular truncation scheme employed is that it assumes that, in addition to contributions which violate quark-hadron duality, also OPE contributions of dimension $D > 8$ unsuppressed by nonleading powers of $\alpha_s$ can be safely neglected. Given the goal of extracting $\alpha_s(m_\tau^2)$ with the best possible accuracy, these features of what we will refer to as the "standard analysis" have been questioned, starting with the work of Refs. [10,11]. In these works, it was argued that both the OPE truncation to terms with $D \leq 8$ and the neglect of violations of quark-hadron duality lead to additional numerically non-negligible systematic uncertainties not included in the errors obtained on $\alpha_s(m_\tau^2)$ and the OPE condensates from the standard-analysis approach. In order to remedy this situation, in Refs. [12,13], we developed a new analysis strategy designed to take both OPE and duality-violating (DV) nonperturbative effects consistently into account. This strategy was then successfully applied to the OPAL data [12,13]. In the present article, we apply this analysis strategy to the corrected ALEPH data, and compare our results to those obtained from the OPAL data in Ref. [13] as well as to those of the recent reanalysis presented in Ref. [1].

The calculation of the order-$\alpha_s^4$ term [14] in the perturbative expansion of the Adler function in 2008 led to a renewed interest in the determination of the strong coupling from hadronic $\tau$ decays, with many attempts to use this new information on the theory side of the relevant FESRs in order to sharpen the extraction of $\alpha_s(m_\tau^2)$ from the data [1,4,10,12–19]. Since the perturbative series converges rather slowly, different partial resummation schemes have been considered, leading to variations in the obtained results. The majority of these post-2007

[1]The updated and corrected data can be found at http://aleph.web.lal.in2p3.fr/tau/specfun13.html.

 

updates (Refs. [1,4,14–19]), however, were carried out assuming that the standard-analysis treatment of nonperturbative effects was essentially correct, with none of the references in this subset, with the exception of Refs. [1,4], redoing the analysis starting from the underlying experimental data (the emphasis, instead, being on the merits of different resummation schemes for the perturbative expansion). Reference [10], which did revisit the determination of the higher-$D$ OPE contributions, and performed a more careful treatment of these contributions, did not, however, include DV contributions in its analysis framework. While its results were tested for self-consistency, the absence of a representation of DV effects meant no estimate of the residual systematic error associated with their neglect was possible. The only articles to incorporate both the improved treatment of higher-$D$ OPE contributions and an implementation of a physically motivated representation of DV effects were those of Refs. [12,13], which, due to the problem with the then-existing ALEPH covariance matrices, were restricted to analyzing OPAL data. Our goal in this article is to reconsider the treatment of nonperturbative effects employing the newly released ALEPH data, which have significantly smaller errors than the OPAL data. We will present results for the two most popular resummation schemes for the perturbative (i.e., $D = 0$ OPE) series: fixed-order perturbation theory (FOPT) and contour-improved perturbation theory (CIPT) [20], without trying to resolve the discrepancies that arise between them (for an overview of the two methods, see Ref. [21]).

This article is organized as follows. In Sec. II we give a brief overview of the necessary theory, referring to Ref. [12] for more details. In Sec. III we discuss the new ALEPH data set, and check explicitly that the current publicly posted version of the correlation matrices pass the test that led to the identification of the problem with the previous version [2]. We also show the comparison of the experimental ALEPH and OPAL nonstrange spectral functions. Section IV summarizes our fitting strategy, developed in Refs. [12,13]. Sections V and VI present the details of the fits, and the results we obtain from them for $\alpha_s(m_\tau^2)$ and dimension 6 and 8 OPE coefficients in the $V$ and $A$ channels. We explore the $\chi^2$ landscape using the Markov-chain Monte Carlo code HROTHGAR [22], which in the case of the OPAL data proved useful in uncovering potential ambiguities. Also included is an estimate for the total nonperturbative contribution to the ratio of nonstrange hadronic and electronic $\tau$ branching fractions. In Sec. VI we check how well the two Weinberg sum rules [23] and the sum rule for the electromagnetic pion mass difference [24] are satisfied by our results. Finally, in Sec. VII, we present a critical discussion of the standard analysis employed in Refs. [1,3,4,8], focusing on the most recent of these, described in Ref. [1]. We demonstrate explicitly the inconsistency of this analysis with regard to the treatment of nonperturbative effects, and conclude that, while the standard analysis approach was a reasonable one to attempt in the past, it must be abandoned in current or future determinations of $\alpha_s(m_\tau^2)$ from hadronic $\tau$ decay data. In our concluding section, Sec. VIII, we compare our approach with the standard-analysis method, highlighting and juxtaposing the assumptions underlying each, and summarize our results.

## II. THEORY OVERVIEW

The sum-rule analysis starts from the correlation functions

$$\begin{aligned}\Pi_{\mu\nu}(q) &= i\int d^4x e^{iqx}\langle 0|T\{J_\mu(x)J_\nu^\dagger(0)\}|0\rangle \\ &= (q_\mu q_\nu - q^2 g_{\mu\nu})\Pi^{(1)}(q^2) + q_\mu q_\nu \Pi^{(0)}(q^2) \\ &= (q_\mu q_\nu - q^2 g_{\mu\nu})\Pi^{(1+0)}(q^2) + q^2 g_{\mu\nu}\Pi^{(0)}(q^2),\end{aligned} \tag{2.1}$$

where $J_\mu$ stands for the nonstrange $V$ or $A$ current, $\bar{u}\gamma_\mu d$ or $\bar{u}\gamma_\mu\gamma_5 d$, while the superscripts (0) and (1) label spin. The decomposition in the third line employs the combinations $\Pi^{(1+0)}(q^2)$ and $q^2\Pi^{(0)}(q^2)$, which are free of kinematic singularities. Defining $s = q^2 = -Q^2$ and the spectral function

$$\rho^{(1+0)}(s) = \frac{1}{\pi}\mathrm{Im}\Pi^{(1+0)}(s), \tag{2.2}$$

Cauchy's theorem and the analytical properties of $\Pi^{(1+0)}(s)$, applied to the contour in Fig. 1, imply the FESR

$$\begin{aligned}I_{V/A}^{(w)}(s_0) &\equiv \frac{1}{s_0}\int_0^{s_0} ds w(s)\rho_{V/A}^{(1+0)}(s) \\ &= -\frac{1}{2\pi i s_0}\oint_{|s|=s_0} ds w(s)\Pi_{V/A}^{(1+0)}(s),\end{aligned} \tag{2.3}$$

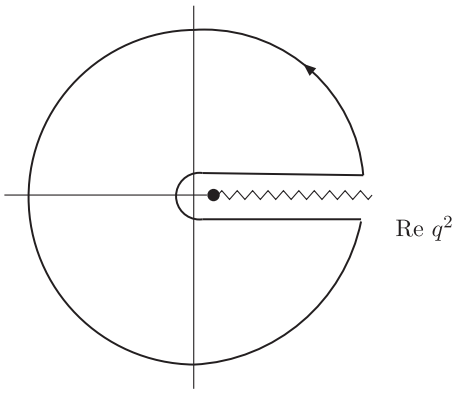


FIG. 1. Analytic structure of $\Pi^{(1+0)}(q^2)$ in the complex $s = q^2$ plane. There is a cut on the positive real axis starting at $s = q^2 = 4m_\pi^2$ (a pole at $s = q^2 = m_\pi^2$ and a cut starting at $s = 9m_\pi^2$) for the $V$ ($A$) case. The solid curve shows the contour used in Eq. (2.3).

valid for any $s_0 > 0$ and any weight $w(s)$ analytic inside and on the contour [5].

The flavor $ud$ $V$ and $A$ spectral functions can be experimentally determined from the differential versions of the ratios,

$$R_{V/A;ud} = \frac{\Gamma[\tau \to (\text{hadrons})_{V/A;ud}\nu_\tau(\gamma)]}{\Gamma[\tau \to e\bar{\nu}_e\nu_\tau(\gamma)]}, \tag{2.4}$$

of the width for hadronic decays induced by the relevant current to that for the electron mode. Explicitly [25],

$$\frac{dR_{V/A;ud}(s)}{ds} = 12\pi^2|V_{ud}|^2 S_{\text{EW}} \frac{1}{m_\tau^2}\left[w_T(s;m_\tau^2)\rho^{(1+0)}_{V/A;ud}(s) - w_L(s;m_\tau^2)\rho^{(0)}_{V/A;ud}(s)\right], \tag{2.5}$$

where $S_{\text{EW}}$ is a short-distance electroweak correction and $w_T(s;s_0) = (1-s/s_0)^2(1+2s/s_0)$, $w_L(s;s_0) = 2(s/s_0)(1-s/s_0)^2$. Apart from the pion-pole contribution, which is not chirally suppressed, $\rho^{(0)}_{V/A;ud}(s) = O[(m_d \mp m_u)^2]$, and the continuum part of $\rho^{(0)}_{V/A}(s)$ is thus numerically negligible. As a result, the spectral functions $\rho^{(1+0)}_{V/A;ud}(s)$ can be determined directly from $dR_{V/A;ud}(s)/ds$. The FESR (2.3) can thus be studied for arbitrary $s_0$ and arbitrary analytic weight $w(s)$. From now on, we will denote the experimental version of the spectral integral on the left-hand side of Eq. (2.3) by $I^{(w)}_{V/A;\text{ex}}(s_0)$ [generically, $I^{(w)}_{\text{ex}}(s_0)$] and the theoretical representation of the contour integral on the right-hand side by $I^{(w)}_{V/A;\text{th}}(s_0)$ [generically, $I^{(w)}_{\text{th}}(s_0)$].

For large enough $|s| = s_0$, away from the positive real axis, $\Pi^{(1+0)}(s)$ can be approximated by the OPE

$$\Pi^{(1+0)}_{\text{OPE}}(s) = \sum_{k=0}^{\infty} \frac{C_{2k}(s)}{(-s)^k}, \tag{2.6}$$

with the OPE coefficients $C_{2k}$ logarithmically dependent on $s$ through perturbative corrections. The term with $k = 0$ corresponds to the purely perturbative, mass-independent contributions, which have been calculated to order $\alpha_s^4$ in Ref. [14], and are the same for the $V$ and $A$ channels. The $C_{2k}$ with $k \geq 1$ are different for the $V$ and $A$ channels, and, for $k > 1$, contain nonperturbative $D = 2k$ condensate contributions. As in Refs. [12,13], we will neglect purely perturbative quark-mass contributions to $C_2$ and $C_4$, as they are numerically very small for the nonstrange FERSs we consider in this article. For the same reason, we will neglect the $s$ dependence of the coefficients $C_{2k}$ for $k > 1$. For the perturbative contribution, $C_0$, we will use the result of Ref. [14] and extract $\alpha_s(m_\tau^2)$ in the $\overline{\text{MS}}$ scheme. Since the coefficient $c_{51}$ of the order-$\alpha_s^5$ term has not been calculated we will use the estimate $c_{51} = 283$ of Ref. [15] with a 100% uncertainty. We will also employ both FOPT and CIPT resummation schemes in evaluating the truncated perturbative series. For more details on the treatment of the $D > 0$ OPE contributions, we refer the reader to Ref. [12].

Perturbation theory, and in general the OPE, breaks down near the positive real $s = q^2$ axis [26]. We account for this by replacing the right-hand side of Eq. (2.3) by

$$-\frac{1}{2\pi i s_0}\oint_{|s|=s_0} ds w(s)(\Pi^{(1+0)}_{\text{OPE}}(s) + \Delta(s)), \tag{2.7}$$

with

$$\Delta(s) \equiv \Pi^{(1+0)}(s) - \Pi^{(1+0)}_{\text{OPE}}(s), \tag{2.8}$$

where the difference $\Delta(s)$ accounts, by definition, for the quark-hadron duality violating contribution to $\Pi^{(1+0)}(s)$. As shown in Ref. [11], Eq. (2.7) can be rewritten as

$$I^{(w)}_{\text{th}}(s_0) = -\frac{1}{2\pi i s_0}\oint_{|s|=s_0} ds w(s)\Pi^{(1+0)}_{\text{OPE}}(s) - \frac{1}{s_0}\int_{s_0}^{\infty} ds w(s)\frac{1}{\pi}\text{Im}\Delta(s), \tag{2.9}$$

if $\Delta(s)$ is assumed to decay fast enough as $s \to \infty$. The imaginary parts $\frac{1}{\pi}\text{Im}\Delta_{V/A}(s)$ can be interpreted as the DV parts, $\rho^{\text{DV}}_{V/A}(s)$, of the $V/A$ spectral functions.

The functional form of $\Delta(s)$ is not known, even for large $s$, and we thus need to resort to a model in order to account for DVs. Following Refs. [11,27,28],[2] we use a model based on large-$N_c$ and Regge considerations, choosing to parametrize $\rho^{\text{DV}}_{V/A}(s)$ as[3]

$$\rho^{\text{DV}}_{V/A}(s) = e^{-\delta_{V/A}-\gamma_{V/A}s}\sin(\alpha_{V/A} + \beta_{V/A}s). \tag{2.10}$$

This introduces, in addition to $\alpha_s$ and the $D \geq 4$ OPE condensates, four new parameters in each channel. As in Refs. [12,13], we will assume that Eq. (2.10) holds for $s \geq s_{\text{min}}$, with $s_{\text{min}}$ to be determined from fits to the data. This, in turn, assumes that we can take $s_{\text{min}}$ significantly smaller than $m_\tau^2$, i.e., that both the OPE and the ansatz (2.10) can be used in some interval below $m_\tau^2$.

Let us pause at this point to revisit the basic ideas underlying the DV ansatz (2.10). Since there exists, as yet, no theory of DVs starting from first principles in QCD, the ansatz (2.10) represents simply our best, physically motivated, guess as to an appropriate form of DV contributions to the $V$ and $A$ spectral functions. The damped oscillatory form employed is, however, far from arbitrary. First, it reflects the fact that DVs are expected to produce almost

[2]See also Refs. [29,30].

[3]In Ref. [12] we used $\kappa_{V/A} \equiv e^{-\delta_{V/A}}$; in Ref. [13] we switched to $\delta_{V/A}$.

harmonic oscillations around the perturbative continuum, in line with expectations from Regge theory, in which resonances occur with equal squared-mass spacings on the relevant daughter trajectories. Second, the exponential damping factor in the ansatz reflects the understanding that the OPE is (at best) an asymptotic, and not a convergent, expansion. It is certainly the case that the OPE representation is more successful for Euclidean $Q^2 \sim 2\ \mathrm{GeV}^2$ than for comparable Minkowski scales, $q^2 \sim 2\ \mathrm{GeV}^2$, where DV contributions are clearly visible in the spectral functions. Once DVs are identified as representing the irreducible error present in this asymptotic expansion, it is natural to assume that their contribution should exhibit an exponentially suppressed dependence on $s = q^2$, as in our ansatz (2.10). These qualitative expectations are also reflected in the explicit Regge- and large-$N_c$-motivated model discussed in much more detail in Refs. [11,27–30]. These plausibility arguments aside, we will use the precise ALEPH data to subject the parametrization (2.10) to nontrivial tests described in detail in Sec. VII.

Several considerations underlie our choice of weight functions $w(s)$. First, we will choose weight functions which are likely to be well behaved in perturbation theory, based on the findings of Ref. [31]. In particular, we will exclude weight functions with a term linear in $s$, and require the ones we use to include a constant term (which we will normalize to one). Second, because it is not known at which order the OPE might start to diverge (for the values of $s_0$ of interest), we wish to avoid terms in Eq. (2.6) with $D > 8$, about which essentially nothing is known. That means that if we do not want to arbitrarily set the coefficients $C_D$ with $D > 8$ equal to zero, our weight functions are restricted to polynomials with degree not larger than 3. Combining these constraints, we are left with the form

$$w(s; s_0) = 1 + a(s/s_0)^2 + b(s/s_0)^3. \tag{2.11}$$

This allows us at most three independent weight functions, and limits the extent to which we can use sufficiently pinched weights, i.e., weights with a (multiple) zero at $s = s_0$, which help to suppress DVs [32,33]. The upshot is that, if we want to exploit the $s_0$ dependence of the data (instead of fitting only at $s_0 = m_\tau^2$, as was done in Refs. [1,3,4,8]) and treat the OPE consistently, modeling DVs is unavoidable [12]. We emphasize that the $s_0$ dependence of fit results provides a crucial test of the validity of FESR fits to the data, as we will see below. As in Refs. [12,13], we choose to consider the weight functions

$$\begin{aligned}
&\hat{w}_0(x) = 1,\\
&\hat{w}_2(x) = 1 - x^2,\\
&\hat{w}_3(x) = (1-x)^2(1+2x) = 1 - 3x^2 + 2x^3 = w_T(s; s_0),\\
&\qquad x \equiv s/s_0.
\end{aligned} \tag{2.12}$$

The first choice, $\hat{w}_0$, is predicated on the fact that pinching is known to suppress DV contributions and we need at least one weight which is sufficiently sensitive to DV contributions to fix the DV parameters. The remaining two weights $\hat{w}_2$ and $\hat{w}_3$ are singly and doubly pinched, respectively. For a more detailed discussion of our choices, we refer to Ref. [12]. An important observation is that these choices for what goes into the parametrization of $I^{(w)}_{\mathrm{th}}(s_0)$ did remarkably well in the analysis of the OPAL data. It therefore makes sense to see what happens if we apply the same strategy to the ALEPH data.

## III. THE ALEPH DATA

In this section, we discuss the revised ALEPH data, which are available from Ref. [34]. First, we perform a minor rescaling, in order to account for more precise values of some "external" quantities (i.e., quantities not directly measured by ALEPH, but used in their analysis of the data); this is discussed in Sec. III A, where we also specify our other inputs. Then, in Sec. III B we apply to the corrected covariance matrices the test of Ref. [2] that led us to uncover the problem with the previously published versions, and verify that the revised covariances pass this test. Finally, we compare the $V$ and $A$ spectral functions obtained from the ALEPH data with those from the OPAL data.

### A. Data and normalization

We will use the following input values in our analysis:

$$\begin{aligned}
m_\tau &= 1.77682(16)\ \mathrm{GeV},\\
B_e &= 0.17827(40),\\
V_{ud} &= 0.97425(22),\\
S_{\mathrm{EW}} &= 1.0201(3),\\
m_\pi &= 139.57018(35)\ \mathrm{MeV},\\
f_\pi &= 92.21(14)\ \mathrm{MeV}.
\end{aligned} \tag{3.1}$$

Here $B_e$ is the branching fraction for the decay $\tau \to e\bar{\nu}_e\nu_\tau$ and we have used the result of a HFAG fit of the $\tau$ branching fractions which incorporates $\pi_{\mu 2}$ and $K_{\mu 2}$ data and Standard Model expectations based on these data for the $\pi$ and $K$ branching fractions [35]; $f_\pi$ is the $\pi$ decay constant. The value for $V_{ud}$ is from Ref. [36], that for $S_{\mathrm{EW}}$ from Ref. [37], and the values for $m_\tau$, $m_\pi$ and $f_\pi$ are from the Particle Data Group [38]. Only the error on $B_e$ has a significant effect in our analysis; errors on the other input quantities are too small to affect the final analysis errors in any significant way.

To the best of our knowledge, Ref. [1] uses the values $B_e = 0.17818(32)$ and $S_{\mathrm{EW}} = 1.0198$. This value for $B_e$ we infer from the ALEPH values for $R_V = 1.782(9)$ [1] and the corresponding branching fraction $B_V = 0.31747$

[34] specified in the publicly posted $V$ data file (no error quoted). The continuum (pion-less) axial branching fraction $B_{A,\mathrm{cont}} = 0.19369$ with $B_e = 0.17818$ translates into $R_{A,\mathrm{cont}} = 1.08705$. From these values, and the quoted value $R_{ud} = 3.475(11)$ [1], it follows that the ALEPH value for $R_\pi$, the pion-pole contribution to $R_{ud}$, is $R_\pi = 0.606$. However, if one employs the very precisely known value of $f_\pi$ quoted above, obtained from $\pi_{\mu 2}$ decays, together with the quoted values for $S_{\mathrm{EW}}$ and $V_{ud}$, one finds instead the more precisely determined expectation $R_\pi = 0.6101$. Using this latter value as well as the ALEPH value $R_{ud} = 3.475(11)$ leads to $R_V + R_{A,\mathrm{cont}} = 2.865$, instead of the ALEPH value $(B_V + B_{A,\mathrm{cont}})/B_e = (0.31747 + 0.19369)/0.17818 = 2.8688$. We employ the more precise $\pi_{\mu 2}$ expectation for the important $A$-channel pion-pole contribution, and take this difference into account by rescaling the $V$ and continuum $A$ nonstrange spectral functions by the common factor $2.865/2.8688 = 0.9987$, since we have no information on whether this rescaling should affect the $V$ and $A$ channels asymmetrically. Our rescaling is thus imperfect, but it is to be noted that the effect of this rescaling lowers our value for $\alpha_s(m_\tau^2)$ by less than one percent, a much smaller shift than that allowed by the total error, see Sec. VI.

The new ALEPH data use a variable bin width, with the highest bin, number 80, centered at $\mathsf{sbin}(80) = 3.3375\,\mathrm{GeV}^2$, which is above $m_\tau^2 = 3.1571\,\mathrm{GeV}^2$. The next-highest bin, number 79, is centered at $\mathsf{sbin}(79) = 3.0875\ \mathrm{GeV}^2$, with a width $\mathsf{dsbin}(79) = 0.1750\ \mathrm{GeV}^2$, so that also $\mathsf{sbin}(79) + \mathsf{dsbin}(79)/2 > m_\tau^2$. In order to avoid using values of $s$ larger than $m_\tau^2$, we will modify these values to

$$\begin{aligned} \mathsf{sbin}(79) &= 3.07854\ \mathrm{GeV}^2, \\ \mathsf{dsbin}(79) &= 0.157089\ \mathrm{GeV}^2, \end{aligned} \tag{3.2}$$

so that $\mathsf{sbin}(79) + \mathsf{dsbin}(79)/2 = m_\tau^2$.

Finally, ALEPH provides binned spectral data for $\mathsf{sfm2}(\mathsf{sbin})$, which are related to the spectral functions by

$$\begin{aligned} \mathsf{sfm2}(\mathsf{sbin}) = 100 \times \frac{12\pi^2 |V_{ud}|^2 S_{\mathrm{EW}} B_e}{m_\tau^2} \\ \times \Delta w^T(\mathsf{sbin}; m_\tau^2) \rho^{(1+0)}(\mathsf{sbin}), \end{aligned} \tag{3.3}$$

in which

$$\Delta w^T(\mathsf{sbin}; m_\tau^2) = \int_{\mathsf{sbin}-\mathsf{dsbin}/2}^{\mathsf{sbin}+\mathsf{dsbin}/2} ds w^T(s; m_\tau^2). \tag{3.4}$$

For infinitesimal $\mathsf{dsbin} = ds$ one has $\Delta w^T(s; m_\tau^2) = w^T(s; m_\tau^2) ds$, but for finite bin width we have to make a choice in how we construct moments with other weights from the spectral functions obtained from Eq. (3.3). We choose to use the definition

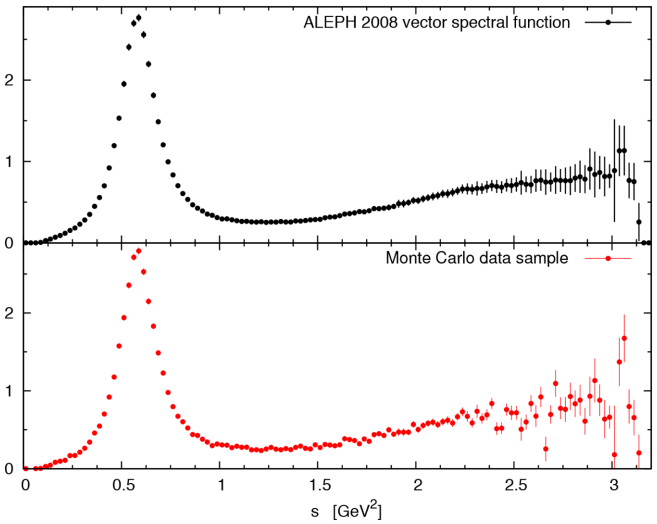


FIG. 2 (color online). Vector spectral function times $2\pi^2$. (Top panel) ALEPH data from 2008 [4]. (Bottom panel) Monte Carlo sample with 2008 covariance matrix.

$$I_{\mathrm{ex}}^{(w)}(s_0) = \sum_{\mathsf{sbin} \le s_0} \left( \int_{\mathsf{sbin}-\mathsf{dsbin}/2}^{\mathsf{sbin}+\mathsf{dsbin}/2} ds w(s; s_0) \right) \rho^{(1+0)}(\mathsf{sbin}) \tag{3.5}$$

for all moments considered in this article.

### B. Correlations

As shown in Ref. [2], there was a problem with the publicly posted 2005 and 2008 versions of the ALEPH covariance matrices. This problem, since corrected in Ref. [1], turns out to have resulted from an inadvertent omission of contributions to the correlations between different bins induced by the unfolding procedure. The problem was discovered by producing fake data sets from a multivariate Gaussian distribution based on the posted ALEPH data and covariance matrices, and then comparing the resulting fake data to the actual ALEPH data. The result of this test is shown in Fig. 2, which is the same as Fig. 3 of Ref. [2]. The top panel shows the experimental data taken from Ref. [4], the bottom panel a typical fake data set produced using the corresponding covariance matrix. The absence of the strong correlations seen in the actual data from the corresponding fake data is what signals the existence of the problem with the previous version of the ALEPH covariance matrix. Figure 3 shows the result of performing the same test on the updated and corrected results reported in Ref. [1], the top panel again showing the actual ALEPH data and the bottom panel a typical fake data set. The fake data (red points) obviously behave much more like the corresponding real data than was the case previously.[4] We have examined many such fake data

[4]Even though the new wider binning near the kinematic end point makes it somewhat harder to see such differences in this region.

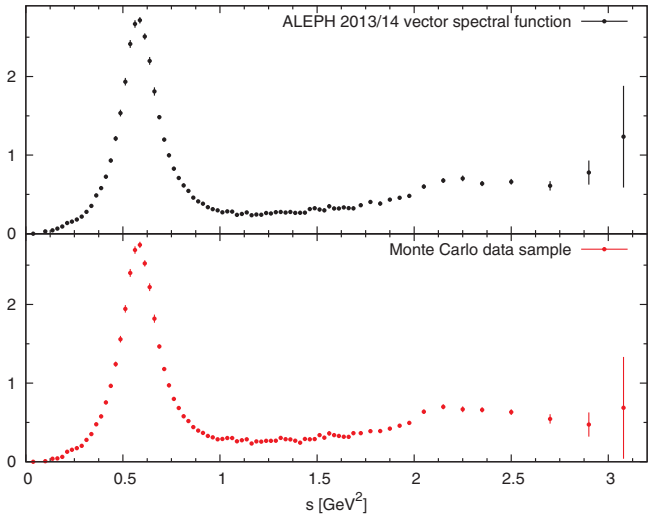


FIG. 3 (color online). Vector spectral function times $2\pi^2$. (Top panel) ALEPH data from 2013 [1]. (Bottom panel) Monte Carlo sample with 2013 covariance matrix.

sets with the same conclusion. A similar exercise was, of course, carried out for the $A$-channel case.

### C. Comparison with OPAL data

In Fig. 4 we show the vector and axial spectral functions as measured by ALEPH [1,34] and OPAL [8]. The normalizations of the spectral functions for both experiments have been updated to take into account modern values for relevant branching fractions; for the normalization of ALEPH data, see Sec. III A above, and for the normalization of OPAL data, see Sec. III of Ref. [13].

While there is in general good agreement between the ALEPH and OPAL spectral functions, a detailed inspection reveals some tension between the two, given the size of the errors, for instance in the regions below 0.5 GeV$^2$ and around 2 GeV$^2$ in the vector channel, with possibly anticorrelated tensions in the same regions in the axial channel. The presence of a large $D = 0$, 1-loop $\alpha_s$-independent contribution in the weighted OPE integrals enhances the impact of such small discrepancies on the output $\alpha_s(m_\tau^2)$. We quantify the impact of these differences below, showing that they lead to some tension between the values for $\alpha_s(m_\tau^2)$ obtained from the two data sets, though the results turn out to agree within total estimated errors.

## IV. FITTING STRATEGY

As already explained in Sec. II, and in more detail in Refs. [12,13], nonpinched weights are needed in order to get a handle on the DV parameters of Eq. (2.10). The simplest and most robust choice of weight allowing us to extract these parameters is the weight $\hat{w}_0(x) = 1$. In order to check the stability of these simple fits, we also perform simultaneous fits of the weights $\hat{w}_0$ and $\hat{w}_2$, and of $\hat{w}_0$, $\hat{w}_2$ and $\hat{w}_3$, as in Refs. [12,13]. This gives us access to the

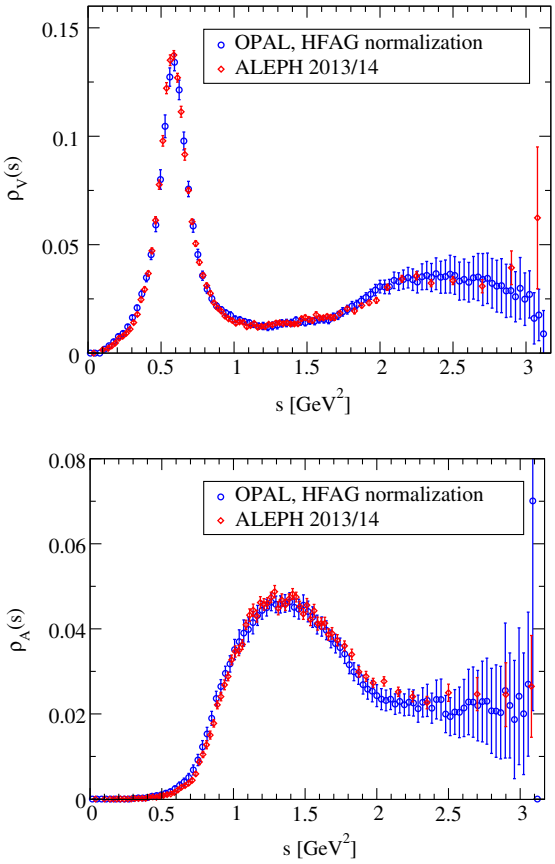


FIG. 4 (color online). Comparison of ALEPH and OPAL data for the spectral functions. (Top panel) $I = 1$ vector channel. (Bottom panel) $I = 1$ continuum (pion-pole subtracted) axial channel.

$D = 6$ and $D = 8$ terms in the OPE, but also allows us to test for the consistency of the values of $\alpha_s(m_\tau^2)$ and the DV parameters between our different fits.

The values we obtain for $I_{\rm ex}^{(w)}(s_0)$ from the ALEPH data are highly correlated, both between different values of $s_0$ and between different weight functions. If we consider only fits using $I_{\rm ex}^{(\hat{w}_0)}(s_0)$ for a range of $s_0$ values, it turns out that fully correlated $\chi^2$ fits are possible, but if we also include $I_{\rm ex}^{(\hat{w}_2)}(s_0)$ and $I_{\rm ex}^{(\hat{w}_3)}(s_0)$ in the fits, the complete correlation matrices become too singular. For fits with multiple weights, we will follow Refs. [12,13], using instead the block-diagonal "fit quality"

$$\mathcal{Q}^2 = \sum_w \sum_{s_0^i, s_0^j} (I_{\rm ex}^{(w)}(s_0^i) - I_{\rm th}^{(w)}(s_0^i; \vec{p}))(C^{(w)})_{ij}^{-1} \times (I_{\rm ex}^{(w)}(s_0^j) - I_{\rm th}^{(w)}(s_0^j; \vec{p})), \tag{4.1}$$

where we have made the dependence of $I_{\rm th}^{(w)}$ on the fit parameters $\vec{p}$ explicit. The matrix $C^{(w)}$ is the (block-diagonal) covariance matrix of the set of moments with fixed weight $w$ and $s_0$ running over the chosen fit window range. The sums over $s_0^i$ and $s_0^j$ are over bins $i$ and $j$, and the

sum over $w$ is over $\hat{w}_0$ and $\hat{w}_2$, or over $\hat{w}_0$, $\hat{w}_2$ and $\hat{w}_3$.[5] The motivation for this choice is that the cross-correlations between two moments arise mainly because the weight functions used in multiple-moment fits appear to be close to being linearly dependent in practice (even though, as a set of polynomials, of course they are not). This near-linear dependence is possibly caused by the relatively large errors on the data for values of $s$ toward $m_\tau^2$, because it is primarily in this region that the weights $\hat{w}_0$, $\hat{w}_2$ and $\hat{w}_3$ differ from each other.

An important observation is that we can freely choose our fit quality $\mathcal{Q}^2$, as long as errors are propagated taking the full data correlation matrix into account. In our case, we choose to estimate fit errors for fits using Eq. (4.1) by propagating the data covariance matrix through a small fluctuation analysis; for details on how this is done, we refer to the Appendix of Ref. [12]. We note that the fit quality $\mathcal{Q}^2$ does not follow a standard $\chi^2$ distribution, so that no absolute meaning can be attached to the minimum value obtained in a fit of this type.

The theoretical moments $I_{\rm th}^{(w)}(s_0;\vec{p})$ are nonlinear functions of (some of) the fit parameters $\vec{p}$, and it is thus not obvious what the probability distribution of the model parameters looks like. As in Ref. [13], we will therefore also explore the posterior probability distribution of the model parameters, assuming that the input data follow a multivariate Gaussian distribution. In order to map out this probability distribution, we use the same Markov-chain Monte Carlo code HROTHGAR [22] as was used in Ref. [13], to which we refer for more details. The distribution generated by HROTHGAR is proportional to $\exp[-\mathcal{Q}^2(\vec{p})/2]$ on the space of parameters, given the data.

## V. FITS

In this section we present our fits, leaving the discussion of $\alpha_s$ and other parameters obtained from these fits to Sec. VI. We first present fits to moments constructed from the $V$ spectral function only, followed by fits using both the $V$ and $A$ spectral moments. We have considered $\chi^2$ fits to $I_{\rm ex}^{(\hat{w}_0)}$ and combined fits using fit qualities of the form (4.1) to $I_{\rm ex}^{(\hat{w}_0)}$, $I_{\rm ex}^{(\hat{w}_2)}$ and $I_{\rm exp}^{(\hat{w}_3)}$. Below we will show only the $\chi^2$ fits to $I_{\rm ex}^{(\hat{w}_0)}$ and the $\mathcal{Q}^2$ fits to all three moments. The results from $\mathcal{Q}^2$ fits to the two moments $I_{\rm ex}^{(\hat{w}_0)}$ and $I_{\rm ex}^{(\hat{w}_2)}$ are completely consistent with these, and we therefore omit them below in the interest of brevity.

As reviewed above, and discussed in much more detail in Refs. [12,13], the necessity to fit not only OPE parameters, but also DV parameters, makes it impossible to fit spectral moments for the sum of the $V$ and $A$ spectral functions. Already for $I_{\rm ex}^{(\hat{w}_0)}$ this would entail a nine-parameter fit, and with the existing data such fits turn out to be unstable. Reference [1] did perform fits to moments of the $V+A$ spectral function at the price of neglecting duality violations and contributions from $D>8$ terms in the OPE; we will compare our fits with those of Ref. [1] in detail in Sec. VII below.

From Fig. 4, we see that the only "feature" in the $A$ channel is the peak corresponding to the $a_1$ meson. In contrast, the $V$ channel data indicate the existence of more resonancelike features than just the $\rho$ meson peak around $s=0.6\ \text{GeV}^2$, even though the resolution is not good enough to resolve multiple resonances beyond the $\rho$. If we wish to avoid making the assumption that already the lowest peak in each channel is in the asymptotic regime in which the ansatz (2.10) is valid, we should limit ourselves to fits to the $V$ channel only. However, we will present also fits to the combined $V$ and $A$ channels below, and see that the results are consistent with those from fits to only the $V$ channel.

In all cases, we find it necessary to include the moment $\hat{w}_0$ in our fits in order to determine both $\alpha_s(m_\tau^2)$ and the DV parameters. While one might consider fits to the spectral function itself, such fits are found to be insufficiently sensitive to the parameter $\alpha_s(m_\tau^2)$, and hence have not been pursued.[6] Fits involving only pinched moments such as $\hat{w}_2$

[5] If only one weight is included in the sum, $\mathcal{Q}^2$ reverts to the standard $\chi^2$.

[6] It is important to distinguish fits to the spectral function itself from fits to the *moments* of the spectral function; they are quite different. Even in the case of the $\hat{w}_0$ moment, the integral $I_{V;\rm ex}^{(\hat{w}_0)}(s_0)$ contains all the data from threshold to $s_0$ and always includes, in particular, the $\rho$ peak. On the other hand, a fit of the DV ansatz (2.10) to the vector spectrum would probably only include data for $s_0$ between $s_{\rm min}$ and $m_\tau^2$, and, since one needs to choose $s_{\rm min}\gg m_\rho^2$, the $\rho$ peak is clearly excluded. The change in $I_{V/A;\rm ex}^{(\hat{w}_0)}(s_0)$ as $s_0$ is increased from the upper edge of bin $k$ to the upper edge of bin $k+1$ is, of course, equal to the average value of the relevant spectral function, $\rho_{V/A}$, in bin $k+1$. As such, in fits which employ all possible $s_0\geq s_{\rm min}$, the fact that the $s_0$ dependence of $I_{V/A;\rm ex}^{(\hat{w}_0)}(s_0)$ is one of the key elements entering the fit means that spectral function values in the interval $s_{\rm min}\leq s\leq m_\tau^2$ are part of the input, but clearly not the *only* input.
Let us be even more specific. First, as already noted, even for single-weight $\hat{w}_0$ fits, the integral of the experimental spectral function over the region from threshold to $s_{\rm min}$ enters the $\hat{w}_0$ moment for all $s_0$. While this is a region in which the OPE and the DV ansatz are not valid, this additional input turns out to be crucial; fits for both $\alpha_s(m_\tau^2)$ and the DV parameters are not possible without including it. Second, as seen in our previous analysis employing the OPAL data, fit results are not changed if, rather than using integrated data for all available $s_0>s_{\rm min}$, one instead employs a winnowed set thereof in the analysis. For such a winnowed set, it is only the sums of the experimental spectral function values over the bins lying between adjacent winnowed $s_0$, and not the full set of spectral function values in all bins in those intervals, that determine the $s_0$ variation entering the fit. Finally, all of the multiweight fits we employ involve weights, $w(x=s/s_0)$, which are themselves $s_0$ dependent. This means that the $s_0$ dependence of the DV part of the corresponding theory moments results not just from the values of $\rho^{\rm DV}(s)$ in the interval $s_0\leq s\leq m_\tau^2$ (where experimental constraints exist), but also involve $s_0$- and $w(x)$-dependent weighted integrals of the DV ansatz form in the interval from $m_\tau^2$ to $\infty$. It would thus be incorrect to characterize the moment-based fit analysis we employ as in any way representing simply a fit to the experimental spectral functions.

TABLE I. $V$ channel fits to $I_{\rm ex}^{(\hat{w}_0)}(s_0)$ from $s_0 = s_{\rm min}$ to $s_0 = m_\tau^2$. FOPT results are shown above the double line, CIPT below; no $D > 0$ OPE terms included in the fit. $\gamma_V$ and $\beta_V$ in units of GeV$^{-2}$.

| $s_{\rm min}$ (GeV$^2$) | $\chi^2$/dof | $p$-value (%) | $\alpha_s$ | $\delta_V$ | $\gamma_V$ | $\alpha_V$ | $\beta_V$ |
|---|---|---|---|---|---|---|---|
| 1.425 | 33.0/21 | 5 | 0.312(11) | 3.36(36) | 0.66(22) | −0.33(61) | 3.27(33) |
| 1.475 | 29.5/19 | 6 | 0.304(11) | 3.32(41) | 0.70(25) | −1.21(73) | 3.72(39) |
| 1.500 | 29.5/18 | 4 | 0.304(11) | 3.32(41) | 0.70(25) | −1.19(87) | 3.71(45) |
| 1.525 | 29.0/17 | 3 | 0.302(11) | 3.37(43) | 0.68(26) | −1.49(94) | 3.86(48) |
| 1.550 | 24.5/16 | 8 | 0.295(10) | 3.50(50) | 0.62(29) | −2.43(94) | 4.32(48) |
| 1.575 | 23.5/15 | 8 | 0.298(11) | 3.50(47) | 0.62(28) | −2.1(1.0) | 4.15(53) |
| 1.600 | 23.4/14 | 5 | 0.297(12) | 3.50(48) | 0.62(28) | −2.1(1.1) | 4.16(56) |
| 1.625 | 23.4/13 | 4 | 0.298(13) | 3.47(50) | 0.63(28) | −2.0(1.2) | 4.12(62) |
| 1.675 | 23.1/11 | 2 | 0.301(15) | 3.35(60) | 0.68(31) | −1.7(1.4) | 3.96(70) |
| 1.425 | 33.2/21 | 4 | 0.331(15) | 3.20(34) | 0.74(21) | −0.30(61) | 3.24(33) |
| 1.475 | 29.5/19 | 6 | 0.320(14) | 3.16(40) | 0.78(24) | −1.20(73) | 3.70(39) |
| 1.500 | 29.5/18 | 4 | 0.320(15) | 3.16(40) | 0.78(24) | −1.19(87) | 3.69(45) |
| 1.525 | 28.9/17 | 4 | 0.317(14) | 3.22(42) | 0.75(25) | −1.51(93) | 3.85(48) |
| 1.550 | 24.3/16 | 8 | 0.308(13) | 3.36(49) | 0.69(28) | −2.48(93) | 4.33(48) |
| 1.575 | 23.3/15 | 8 | 0.311(14) | 3.35(46) | 0.69(27) | −2.2(1.0) | 4.17(52) |
| 1.600 | 23.3/14 | 6 | 0.311(15) | 3.36(47) | 0.69(27) | −2.2(1.1) | 4.19(56) |
| 1.625 | 23.2/13 | 4 | 0.312(16) | 3.33(49) | 0.70(28) | −2.1(1.2) | 4.15(62) |
| 1.675 | 23.0/11 | 2 | 0.314(19) | 3.23(58) | 0.74(30) | −1.8(1.5) | 4.02(74) |

and $\hat{w}_3$, on the other hand, are insufficiently sensitive to the DV parameters. All our fits will thus include the spectral moments $I_{\rm ex}^{(\hat{w}_0)}(s_0)$, either in the $V$ channel alone or in the combined $V$ and $A$ channels. In the latter case, there is a separate set of DV parameters for each of these channels, but the fit parameter $\alpha_s(m_\tau^2)$ is, of course, common to both.[7]

### A. Fits to vector channel data

We begin with fits to the single moment $I_{\rm ex}^{(\hat{w}_0)}(s_0)$, as a function of $s_{\rm min}$, with $s_{\rm min}$ defined to be the minimum value of $s_0$ included in the fit. Since these are $\chi^2$ fits, one may estimate the $p$-values for these fits; they are shown in the third column of Table I. We note that the $p$-values are not large, but they are not small enough to exclude the validity of our fit function based on the ALEPH data. Judged by $p$-value, the fits with $s_{\rm min} = 1.55$ and 1.575 GeV$^2$ are the best fits, and we thus take the average value of the central values for the fit parameters from these two fits as our best value, with a statistical error that is the larger of the two (noting that these are essentially equal in size). For the strong coupling, we find

$$\begin{aligned} \alpha_s(m_\tau^2) &= 0.296(11) \qquad \text{(FOPT)}, \\ &= 0.310(14) \qquad \text{(CIPT)}. \end{aligned} \tag{5.1}$$

The difference between the FOPT and CIPT results reflects the well-known fact that the two prescriptions show no sign of converging to one another as the truncation order is increased [14,15]. We observe that the $p$-value starts to decrease again from $s_{\rm min} = 1.6$ GeV$^2$, indicating that the data become too sparse for an optimal fit. We investigated the sensitivity of these fits to omitting the data in up to four bins with the largest values of $s$, and found no significant difference. This is no surprise, given the errors shown in Fig. 5. For illustration, we show the parameter correlation matrix for the FOPT fit with $s_{\rm min} = 1.55$ GeV$^2$ in Table II.

In Fig. 5 we show the results of CIPT and FOPT fits to $I_{\rm ex}^{(\hat{w}_0)}(s_0)$ for $s_{\rm min} = 1.55$ GeV$^2$. The left panel shows the results of the fits for the moment, the right-hand panel the OPE + DV versions of the spectral functions resulting from these fits.

TABLE II. Parameter correlation matrix for the $V$ channel $\hat{w}_0$ FOPT fit with $s_{\rm min} = 1.55$ GeV$^2$ shown in Table I.

| | $\alpha_s$ | $\delta_V$ | $\gamma_V$ | $\alpha_V$ | $\beta_V$ |
|---|---|---|---|---|---|
| $\alpha_s$ | 1 | 0.600 | −0.606 | 0.689 | −0.653 |
| $\delta_V$ | 0.600 | 1 | −0.994 | 0.310 | −0.297 |
| $\gamma_V$ | −0.606 | −0.994 | 1 | −0.330 | 0.315 |
| $\alpha_V$ | 0.689 | 0.310 | −0.330 | 1 | −0.996 |
| $\beta_V$ | −0.653 | −0.297 | 0.315 | −0.996 | 1 |

[7]The $D > 2$ OPE coefficients are also generally different between the $V$ and $A$ channels [7]. In the case of $C_4$ (which, due to the absence of terms linear in $x$, does not enter for the weights we employ, in the approximation of dropping contributions higher-than-leading order in $\alpha_s$) the full gluon condensate and leading-order quark condensate contributions are the same for the $V$ and $A$ channels. For polynomial weights with a term linear in $x$, $D = 4$ contributions would be present, and one could impose the resulting near equality of $C_4$ in the $V$ and $A$ channels. This was done in the version of the analysis performed by OPAL but not in the analyses of the ALEPH Collaboration, including Ref. [1]. The fact that the fitted value of the gluon condensate obtained from independent $V$ and $A$ channel fits in Ref. [1] is not close to agreeing within errors is, in fact, a clear sign of the unphysical nature of these fits, see Sec. VII below.

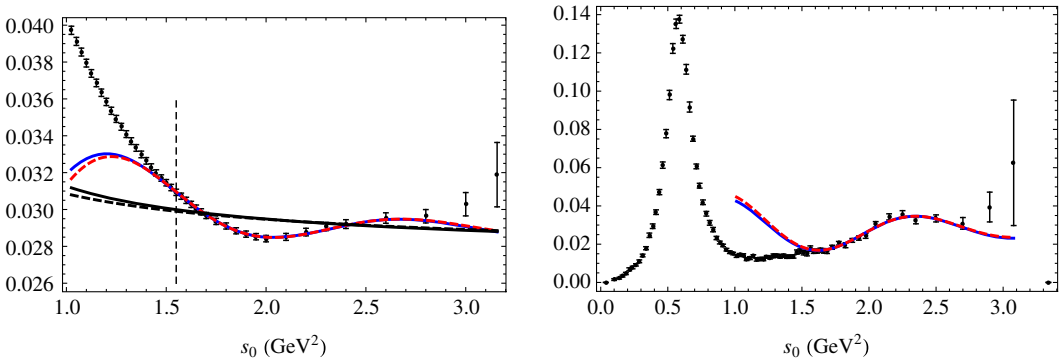


FIG. 5 (color online). (Left panel) Comparison of $I_{\rm ex}^{(\hat{w}_0)}(s_0)$ and $I_{\rm th}^{(\hat{w}_0)}(s_0)$ for the $s_{\rm min} = 1.55$ GeV$^2$ $V$ channel fits of Table I. (Right panel) Comparison of the theoretical spectral function resulting from this fit with the experimental results. CIPT fits are shown in red (dashed lines) and FOPT in blue (solid lines). The (much flatter) black curves in the left panel represent the OPE parts of the fits, i.e., the fit results with the DV parts removed. The vertical dashed line indicates the location of $s_{\rm min}$.

As in Ref. [13], we studied the posterior probability distribution, using the same Markov-chain Monte Carlo code, HROTHGAR [22]. We remind the reader that it is not obvious what this distribution looks like, even if we assume that the data errors follow a multivariate Gaussian distribution. For the fits of Table I, this code generates points in the five-dimensional parameter space, and computes the $\chi^2$ value associated with each of these points. These points are distributed as $\exp[-\chi^2(\vec{p})]$, with $\vec{p}$ the parameter vector, and $\chi^2$ evaluated on the ALEPH data (including the full covariance matrix) and the values of the parameters at these points.

In Fig. 6 we show $\chi^2$ as a function of $\alpha_s(m_\tau^2)$, choosing the FOPT fit with $s_{\rm min} = 1.55$ GeV$^2$. Since for each $\alpha_s(m_\tau^2)$ points with many different values for the other four parameters are generated stochastically, the distribution appears as the cloud shown in the figure. This distribution shows a unique minimum for the value of $\chi^2$, at approximately $\alpha_s(m_\tau^2) = 0.295$, consistent with Table I. The width of the distribution is also roughly consistent with the error of $\pm 0.010$, but we see that the distribution of points is not entirely symmetric around the minimum. There is no alternative (local) minimum, as was the case with the OPAL data [13].

We also find the parameters $\delta_V$ and $\gamma_V$ to be much better constrained than was the case for the corresponding fits to the OPAL data in Ref. [13]. The distributions in the $\delta_V - \alpha_s(m_\tau^2)$ and $\delta_V - \gamma_V$ planes are shown in the left and right panels of Fig. 7.[8] Since for all other fits presented in the rest of this article the conclusions about the posterior probability distribution found with HROTHGAR are similar, we will refrain from showing the analogues of Figs. 6 and 7 for those fits.

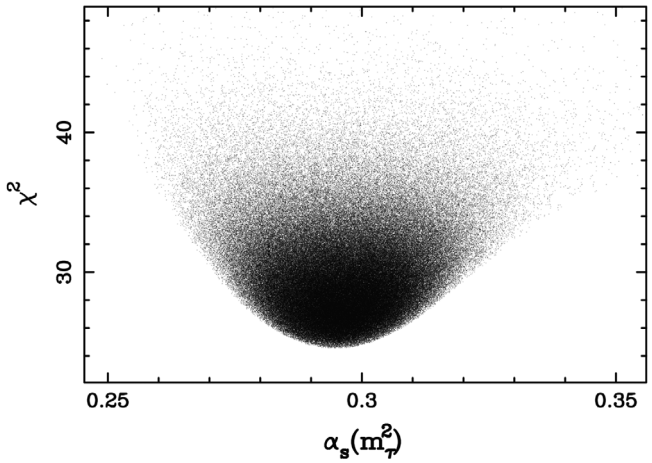


FIG. 6. $\chi^2$ versus $\alpha_s(m_\tau^2)$, FOPT, $s_{\rm min} = 1.55$ GeV$^2$, 1250000 points.

Next, we consider simultaneous fits to the moments $I_{\rm ex}^{(\hat{w}_0)}(s_0)$, $I_{\rm ex}^{(\hat{w}_2)}(s_0)$ and $I_{\rm ex}^{(\hat{w}_0)}(s_3)$; results for the same values of $s_{\rm min}$ as before are given in Table III. These fits are performed by minimizing $\mathcal{Q}^2$ as defined in Eq. (4.1), with correlations between different moments omitted. However, the full correlation matrix, including correlations between different moments, has been taken into account in the parameter fit error estimates shown in the table. These errors were determined by linear propagation of the full data covariance matrix; for a detailed explanation of the method, we refer to the Appendix of Ref. [12].

Judging by the values of $\mathcal{Q}^2/{\rm dof}$,[9] again the two fits for $s_{\rm min} = 1.55$ and $1.575$ GeV$^2$ are the optimal ones. Averaging parameter values between these two fits, we find

[8]Note that the vertical axis covers the interval $\delta_V \in [2, 5]$, to be compared with the significantly larger interval $\delta_V \in [-2, 5]$ in Fig. 2 of Ref. [13].

[9]Which, given the fact that $\mathcal{Q}^2$ is not equal to $\chi^2$ for these fits, cannot easily be translated into $p$-values.

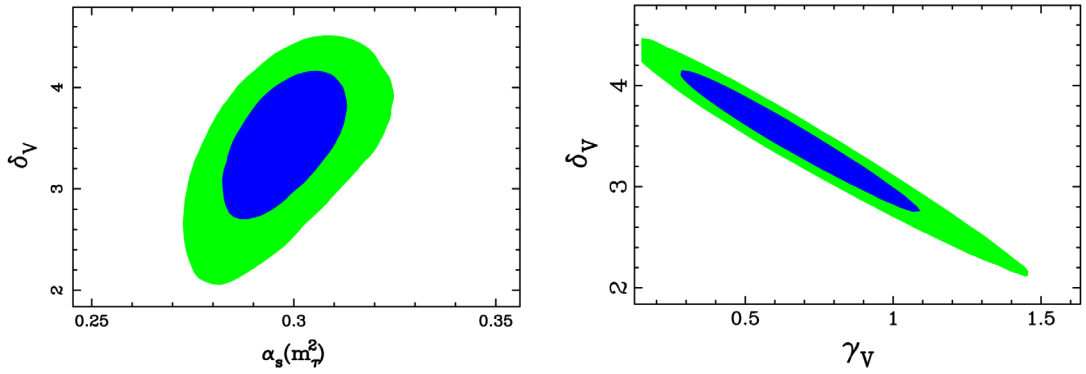


FIG. 7 (color online). Two-dimensional contour plots showing $\delta_V$ versus $\alpha_s(m_\tau^2)$ (left panel) and $\delta_V$ versus $\gamma_V$ (right panel) for the $V$ channel $\hat{w}_0$ FOPT, $s_{\min} = 1.55$ GeV$^2$ fit. Blue (darker) areas and green (lighter) areas contain 68% and 95%, respectively, of the distribution. $\gamma_V$ in units of GeV$^{-2}$.

$$\begin{aligned} \alpha_s(m_\tau^2) &= 0.296(10) \qquad \text{(FOPT)}, \\ &= 0.310(14) \qquad \text{(CIPT)}, \end{aligned} \tag{5.2}$$

in excellent agreement with Eq. (5.1). We have also considered fits involving only the two moments $I_{\rm ex}^{(\hat{w}_0)}(s_0)$ and $I_{\rm ex}^{(\hat{w}_2)}(s_0)$, and find results very similar to those contained in Tables I and III. In Fig. 8 we show the quality of the fits of Table III for $s_{\min} = 1.55$ GeV$^2$.

We end this subsection with several comments. First, we see that pinching indeed serves to suppress the role of DV contributions. The upper right panel in Fig. 8 shows the singly pinched $\hat{w}_2$ case and the lower left panel shows the doubly pinched $\hat{w}_3$ case. There is also a significant difference between the colored and black curves in all panels, though with the onset of this difference shifting to lower $s_0$ as the degree of pinching is increased. The existence of these differences implies that, with the errors on the ALEPH data, the presence of duality violations is evident for all three moments. This, in turn, implies that omitting duality violations from the theory side of the corresponding FESRs has the potential to produce a significant additional systematic error on $\alpha_s(m_\tau^2)$ (and the higher-$D$ OPE coefficients) that cannot be estimated if only fits without DV parameters are attempted. We will return to this point in Sec. VII below. Second, we note that the spectral function itself below $s = s_{\min}$ is not very well described by the curves obtained from the fits. While the form of Eq. (2.10) constitutes a reasonable assumption for asymptotically

TABLE III. $V$ channel fits to $I_{\rm ex}^{(\hat{w}_0)}(s_0)$, $I_{\rm ex}^{(\hat{w}_2)}(s_0)$ and $I_{\rm ex}^{(\hat{w}_0)}(s_3)$ from $s_0 = s_{\min}$ to $s_0 = m_\tau^2$, FOPT results are shown above the double line, CIPT below; $D = 6, 8$ OPE terms included in the fit. $\gamma_V$ and $\beta_V$ in units of GeV$^{-2}$, $C_{6V}$ in units of GeV$^6$ and $C_{8V}$ in units of GeV$^8$.

| $s_{\min}$ (GeV$^2$) | $\mathcal{Q}^2$/dof | $\alpha_s$ | $\delta_V$ | $\gamma_V$ | $\alpha_V$ | $\beta_V$ | $10^2 C_{6V}$ | $10^2 C_{8V}$ |
|---|---|---|---|---|---|---|---|---|
| 1.425 | 106.0/71 = 1.49 | 0.305(10) | 3.02(38) | 0.87(24) | −0.68(56) | 3.43(31) | −0.59(17) | 0.94(29) |
| 1.475 | 93.3/65 = 1.43 | 0.302(10) | 3.07(44) | 0.85(27) | −1.41(68) | 3.81(36) | −0.71(16) | 1.19(28) |
| 1.500 | 93.2/62 = 1.50 | 0.302(10) | 3.08(45) | 0.85(27) | −1.40(77) | 3.80(40) | −0.71(18) | 1.19(30) |
| 1.525 | 85.6/59 = 1.45 | 0.298(10) | 3.21(49) | 0.78(29) | −1.96(78) | 4.08(41) | −0.79(16) | 1.36(27) |
| 1.550 | 76.3/56 = 1.36 | 0.295(10) | 3.30(52) | 0.74(30) | −2.48(81) | 4.33(41) | −0.86(14) | 1.50(24) |
| 1.575 | 74.5/53 = 1.41 | 0.297(10) | 3.29(51) | 0.74(29) | −2.25(87) | 4.22(44) | −0.83(16) | 1.43(27) |
| 1.600 | 74.2/50 = 1.48 | 0.297(11) | 3.31(51) | 0.73(30) | −2.27(92) | 4.23(47) | −0.83(16) | 1.44(29) |
| 1.625 | 73.8/47 = 1.57 | 0.298(11) | 3.28(54) | 0.74(31) | −2.16(99) | 4.18(50) | −0.81(18) | 1.40(32) |
| 1.675 | 72.0/41 = 1.76 | 0.299(12) | 3.28(63) | 0.74(34) | −2.1(1.1) | 4.13(57) | −0.80(21) | 1.37(39) |
| 1.425 | 98.6/71 = 1.39 | 0.328(16) | 3.17(39) | 0.77(25) | −0.43(61) | 3.30(32) | −0.60(19) | 0.83(35) |
| 1.475 | 89.5/65 = 1.38 | 0.319(14) | 3.11(44) | 0.81(27) | −1.24(71) | 3.72(37) | −0.76(16) | 1.18(31) |
| 1.500 | 89.4/62 = 1.44 | 0.319(15) | 3.11(44) | 0.81(27) | −1.20(81) | 3.70(42) | −0.76(18) | 1.16(34) |
| 1.525 | 82.1/59 = 1.39 | 0.314(14) | 3.22(48) | 0.77(28) | −1.81(80) | 4.00(42) | −0.85(15) | 1.37(28) |
| 1.550 | 73.7/56 = 1.32 | 0.309(13) | 3.28(51) | 0.74(30) | −2.39(82) | 4.28(42) | −0.93(13) | 1.53(25) |
| 1.575 | 71.8/53 = 1.35 | 0.311(14) | 3.28(50) | 0.74(29) | −2.12(89) | 4.15(45) | −0.89(15) | 1.45(28) |
| 1.600 | 71.7/50 = 1.43 | 0.311(14) | 3.28(51) | 0.74(29) | −2.16(94) | 4.17(48) | −0.90(15) | 1.46(29) |
| 1.625 | 71.5/47 = 1.52 | 0.312(15) | 3.24(53) | 0.75(30) | −2.0(1.0) | 4.11(51) | −0.88(17) | 1.42(34) |
| 1.675 | 69.8/41 = 1.70 | 0.313(16) | 3.22(63) | 0.76(33) | −1.9(1.2) | 4.04(59) | −0.86(20) | 1.38(42) |

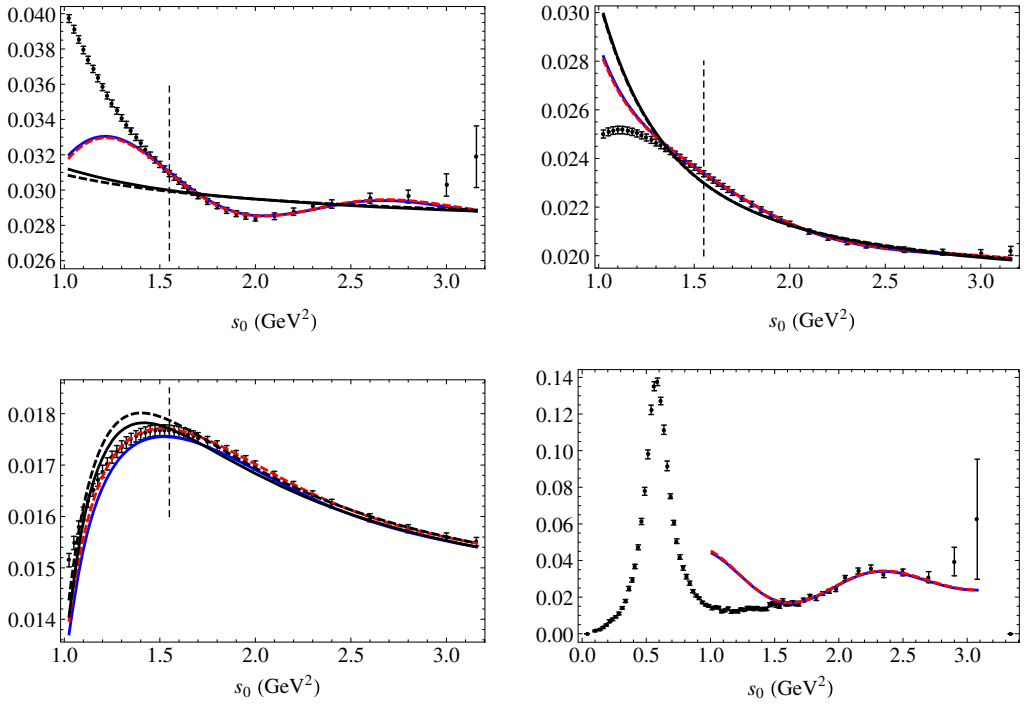


FIG. 8 (color online). (Upper left panel) Comparison of $I^{(\hat{w}_0)}_{\rm ex}(s_0)$ and $I^{(\hat{w}_0)}_{\rm th}(s_0)$ for the $s_{\rm min} = 1.55$ GeV$^2$ $V$ channel fits of Table III. (Lower left and upper right panels) Analogous comparisons for $I^{(\hat{w}_2)}(s_0)$ (upper right panel) and $I^{(\hat{w}_3)}(s_0)$ (lower left panel). CIPT fits are shown in red (dashed) lines and FOPT in blue (solid) lines. (Lower right panel) Comparison of the theoretical spectral function resulting from this fit with the experimental results. The black curves (which are much flatter for the $\hat{w}_0$ case) represent the OPE parts of the fits. The vertical dashed line indicates the location of $s_{\rm min}$.

large $s$, we do not know *a priori* what a reasonable value of $s_{\rm min}$ should be. It is clear, however, that our ansatz works reasonably well for $s \gtrsim 1.5$ GeV$^2$, but that the asymptotic regime definitely does not include the region around the $\rho$ peak.

### B. Combined fits to vector and axial channel data

We now consider fits analogous to those of the preceding subsection, involving simultaneous fitting of the $V$ and $A$ spectral moments as a function of $s_{\rm min}$. The fit parameter $\alpha_s(m_\tau^2)$ is common to the two channels, while the $D > 0$ OPE and DV parameters are distinct for each. Fits to $I^{(\hat{w}_0)}_{{\rm ex},V}(s_0)$ and $I^{(\hat{w}_0)}_{{\rm ex},A}(s_0)$ are shown in Table IV; we displayed fewer values of $s_{\rm min}$ for the sake of brevity.

Fits with $s_{\rm min} = 1.55$ and 1.575 GeV$^2$ have the highest $p$-values, as before. Averaging the parameter values for these fits, we find

$$\begin{aligned} \alpha_s(m_\tau^2) &= 0.299(12) \qquad \text{(FOPT)}, \\ &= 0.313(15) \qquad \text{(CIPT)}, \end{aligned} \tag{5.3}$$

slightly higher values than those of Eqs. (5.1) and (5.2), but consistent within errors. The errors are $\chi^2$ errors, since all correlations were taken into account in the fit; they are slightly larger than those found in the $V$-channel fits.

For $s_{\rm min} = 1.55$ GeV$^2$ we show the quality of the fits in the left panels of Fig. 9 and the $V$ and $A$ spectral-function comparisons obtained using parameter values from the fit in the corresponding right-hand panels. We note that the fit curves in the axial case are essentially determined by the shoulder of the $a_1$ resonance, in contrast to what happens in the vector case, where the $\rho$ peak is well away from the region relevant for the shape of the fit curves.

Table V shows the results of the combined $V$ and $A$ channel fits to the three moments $I^{(\hat{w}_0)}_{\rm ex}(s_0)$, $I^{(\hat{w}_2)}_{\rm ex}(s_0)$ and $I^{(\hat{w}_0)}_{\rm ex}(s_3)$. Judging by the values of $\mathcal{Q}^2$/degrees of freedom (dof), the best fits are again those with $s_{\rm min} = 1.55$ and 1.575 GeV$^2$, leading to

$$\begin{aligned} \alpha_s(m_\tau^2) &= 0.293(9) \qquad \text{(FOPT)}, \\ &= 0.313(13) \qquad \text{(CIPT)}. \end{aligned} \tag{5.4}$$

These values are in good agreement with those of the other fits reported above. As before, fits to just the pair of moments $I^{(\hat{w}_0)}_{\rm ex}(s_0)$ and $I^{(\hat{w}_2)}_{\rm ex}(s_0)$ do not lead to any surprises. We show the quality of the fits of Table V for the moments $I^{(\hat{w}_0)}_{\rm ex}(s_0)$ and the comparison of the resulting spectral functions to the experimental ones for both channels in Fig. 10. The fits for the other two moments

TABLE IV. Combined $V$ and $A$ channel fits to $I_{\rm ex}^{(\hat{w}_0)}(s_0)$ from $s_0 = s_{\rm min}$ to $s_0 = m_\tau^2$. FOPT results are shown above the double line, CIPT below; no $D > 0$ OPE terms are included in the fit. $\gamma_{V,A}$ and $\beta_{V,A}$ in units of GeV$^{-2}$.

| | | | | $\delta_V$ | $\gamma_V$ | $\alpha_V$ | $\beta_V$ |
|---|---|---|---|---|---|---|---|
| $s_{\rm min}$ (GeV$^2$) | $\chi^2$/dof | $p$-value (%) | $\alpha_s$ | $\delta_A$ | $\gamma_A$ | $\alpha_A$ | $\beta_A$ |
| 1.500 | 49.8/37 | 8 | 0.310(14) | 3.45(40) | 0.62(24) | −1.0(1.0) | 3.60(53) |
| | | | | 1.85(38) | 1.38(20) | 4.5(1.2) | 2.46(59) |
| 1.525 | 48.6/35 | 6 | 0.309(15) | 3.53(42) | 0.59(25) | −1.2(1.2) | 3.71(60) |
| | | | | 1.99(40) | 1.31(20) | 4.4(1.2) | 2.49(62) |
| 1.550 | 40.0/33 | 19 | 0.297(11) | 3.57(48) | 0.58(28) | −2.33(97) | 4.27(50) |
| | | | | 1.56(49) | 1.44(22) | 5.43(89) | 1.99(46) |
| 1.575 | 38.7/31 | 16 | 0.300(12) | 3.57(45) | 0.58(26) | −1.9(1.1) | 4.08(55) |
| | | | | 1.67(51) | 1.41(23) | 5.22(94) | 2.10(48) |
| 1.600 | 37.2/298 | 14 | 0.300(12) | 3.56(46) | 0.59(27) | −2.0(1.2) | 4.10(59) |
| | | | | 1.41(57) | 1.52(25) | 5.4(1.0) | 2.01(52) |
| 1.625 | 35.4/27 | 13 | 0.300(13) | 3.50(48) | 0.62(27) | −1.9(1.3) | 4.07(64) |
| | | | | 0.90(72) | 1.73(29) | 5.8(1.2) | 1.82(60) |
| 1.500 | 49.7/37 | 8 | 0.327(18) | 3.29(39) | 0.70(24) | −1.0(1.0) | 3.59(53) |
| | | | | 1.92(39) | 1.35(20) | 4.5(1.1) | 2.50(60) |
| 1.525 | 48.5/35 | 6 | 0.326(19) | 3.37(40) | 0.66(24) | −1.2(1.2) | 3.70(60) |
| | | | | 2.06(41) | 1.28(21) | 4.4(1.2) | 2.54(62) |
| 1.550 | 39.7/33 | 20 | 0.311(13) | 3.43(47) | 0.65(27) | −2.38(96) | 4.28(49) |
| | | | | 1.61(49) | 1.43(22) | 5.36(87) | 2.04(45) |
| 1.575 | 38.4/31 | 17 | 0.315(15) | 3.42(44) | 0.65(26) | −2.0(1.1) | 4.10(56) |
| | | | | 1.72(52) | 1.39(24) | 5.15(92) | 2.14(48) |
| 1.600 | 36.9/29 | 15 | 0.314(15) | 3.41(45) | 0.66(26) | −2.1(1.2) | 4.13(59) |
| | | | | 1.46(58) | 1.50(25) | 5.33(98) | 2.06(51) |
| 1.625 | 35.1/27 | 14 | 0.314(16) | 3.36(48) | 0.68(27) | −2.0(1.3) | 4.11(64) |
| | | | | 0.96(72) | 1.71(29) | 5.7(1.1) | 1.87(58) |

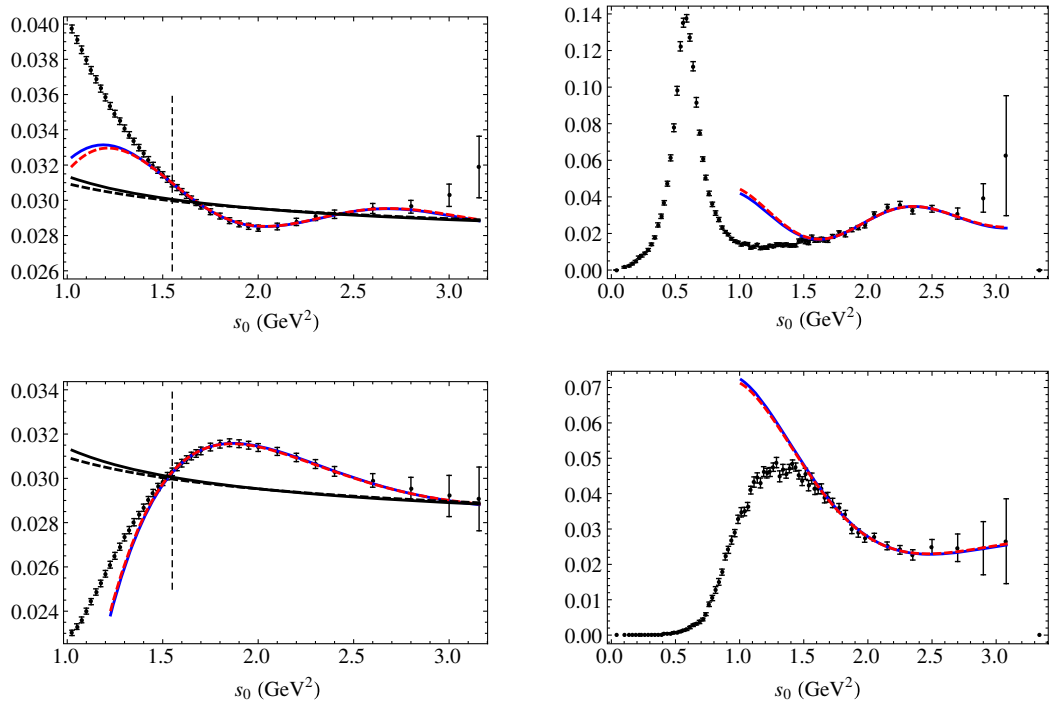


FIG. 9 (color online). (Left panels) Comparison of $I_{\rm ex}^{(\hat{w}_0)}(s_0)$ and $I_{\rm th}^{(\hat{w}_0)}(s_0)$ for the $s_{\rm min} = 1.55$ GeV$^2$ combined $V$ and $A$ channel fits of Table IV ($V$ top, $A$ bottom). (Right panels) Comparison of the theoretical spectral function resulting from this fit with the experimental results ($V$ top, $A$ bottom). CIPT fits are shown in red (dashed) lines and FOPT in blue (solid) lines. The (much flatter) black curves on the left represent the OPE parts of the fits. The vertical dashed line indicates the location of $s_{\rm min}$.

TABLE V. Combined $V$ and $A$ channel fits to $I^{(\hat{w}_0)}_{\rm ex}(s_0)$, $I^{(\hat{w}_2)}_{\rm ex}(s_0)$ and $I^{(\hat{w}_3)}_{\rm ex}(s_0)$ from $s_0 = s_{\rm min}$ to $s_0 = m_\tau^2$. FOPT results are shown above the double line, CIPT below; $D = 6, 8$ OPE terms included in the fit. $\gamma_{V,A}$ and $\beta_{V,A}$ in units of GeV$^{-2}$, $C_{6V,A}$ in units of GeV$^6$ and $C_{8V,A}$ in units of GeV$^8$.

| $s_{\rm min}$ (GeV$^2$) | $\mathcal{Q}^2$/dof | $\alpha_s$ | $\delta_{V,A}$ | $\gamma_{V,A}$ | $\alpha_{V,A}$ | $\beta_{V,A}$ | $10^2 C_{6V,A}$ | $10^2 C_{8V,A}$ |
|---|---|---|---|---|---|---|---|---|
| 1.475 | $182/131 = 1.39$ | 0.297(7) | 2.90(42) | 0.95(26) | −1.61(65) | 3.91(35) | −0.78(13) | 1.31(23) |
| | | | 2.26(35) | 1.13(18) | 4.92(58) | 2.25(30) | −0.08(35) | 1.12(96) |
| 1.500 | $160/125 = 1.28$ | 0.297(8) | 2.92(43) | 0.94(26) | −1.62(73) | 3.91(39) | −0.78(14) | 1.31(25) |
| | | | 1.90(44) | 1.29(21) | 5.26(69) | 2.08(36) | −0.26(44) | 1.8(1.4) |
| 1.525 | $149/119 = 1.25$ | 0.294(8) | 3.08(48) | 0.86(28) | −2.16(75) | 4.18(40) | −0.85(13) | 1.46(23) |
| | | | 1.86(48) | 1.30(22) | 5.38(72) | 2.02(37) | −0.38(49) | 2.1(1.6) |
| 1.550 | $126/113 = 1.11$ | 0.292(9) | 3.19(51) | 0.80(30) | −2.65(79) | 4.42(41) | −0.90(13) | 1.57(22) |
| | | | 1.53(56) | 1.42(24) | 5.73(84) | 1.84(43) | −0.63(61) | 3.0(2.2) |
| 1.575 | $124/107 = 1.16$ | 0.293(9) | 3.18(51) | 0.81(29) | −2.47(84) | 4.33(43) | −0.88(14) | 1.52(24) |
| | | | 1.57(61) | 1.41(26) | 5.67(86) | 1.87(44) | −0.57(61) | 2.8(2.2) |
| 1.600 | $116/101 = 1.15$ | 0.293(9) | 3.20(52) | 0.80(30) | −2.51(89) | 4.35(46) | −0.89(14) | 1.53(25) |
| | | | 1.14(74) | 1.59(29) | 6.0(1.0) | 1.72(53) | −0.73(72) | 3.6(2.7) |
| 1.625 | $112/95 = 1.18$ | 0.294(10) | 3.20(55) | 0.79(31) | −2.43(95) | 4.31(48) | −0.87(15) | 1.50(28) |
| | | | 0.85(92) | 1.71(34) | 6.2(1.2) | 1.61(63) | −0.80(80) | 4.0(3.2) |
| 1.475 | $159/131 = 1.21$ | 0.338(13) | 3.45(32) | 0.61(20) | −0.63(67) | 3.42(35) | −0.58(16) | 0.83(31) |
| | | | 2.23(33) | 1.25(21) | 3.45(81) | 3.02(42) | 0.59(25) | −0.64(58) |
| 1.500 | $146/125 = 1.17$ | 0.328(15) | 3.26(39) | 0.72(24) | −0.92(79) | 3.56(41) | −0.67(18) | 1.00(35) |
| | | | 1.96(41) | 1.34(22) | 4.41(89) | 2.53(46) | 0.25(40) | 0.3(1.0) |
| 1.525 | $136/119 = 1.14$ | 0.320(13) | 3.35(44) | 0.69(26) | −1.59(79) | 3.90(41) | −0.80(15) | 1.26(29) |
| | | | 1.93(46) | 1.32(23) | 4.76(83) | 2.35(43) | 0.05(43) | 0.78(12) |
| 1.550 | $118/113 = 1.04$ | 0.312(13) | 3.35(49) | 0.70(29) | −2.28(81) | 4.23(42) | −0.90(13) | 1.48(25) |
| | | | 1.59(55) | 1.44(25) | 5.37(89) | 2.03(46) | −0.33(56) | 2.0(1.8) |
| 1.575 | $115/107 = 1.07$ | 0.315(13) | 3.35(48) | 0.70(28) | −1.98(88) | 4.09(45) | −0.86(15) | 1.39(29) |
| | | | 1.65(59) | 1.42(27) | 5.23(92) | 2.11(47) | −0.22(55) | 1.6(1.7) |
| 1.600 | $108/101 = 1.07$ | 0.314(14) | 3.33(49) | 0.71(29) | −2.04(93) | 4.12(47) | −0.87(15) | 1.41(30) |
| | | | 1.23(70) | 1.60(30) | 5.6(1.1) | 1.95(55) | −0.37(64) | 2.2(2.2) |
| 1.625 | $105/95 = 1.10$ | 0.315(15) | 3.28(53) | 0.73(30) | −1.9(1.0) | 4.06(51) | −0.85(17) | 1.37(34) |
| | | | 0.96(85) | 1.71(35) | 5.7(1.2) | 1.87(63) | −0.42(71) | 2.4(2.5) |

look very similar to those in Fig. 8 for the $V$ channel, and show a similar quality in the $A$ channel.

## VI. TESTS AND RESULTS

There are a number of consistency checks that can be applied once values for $\alpha_s(m_\tau^2)$ as well as the $D > 0$ OPE and DV parameters have been obtained from a fit. We will present some of these in Sec. VI A. Then, in Sec. VI B, we will present our final number for $\alpha_s(m_\tau^2)$, following this in Sec. VI C by a determination of the nonperturbative contribution to $R_{V+A;ud}$ and a comparison of the $D = 6$ OPE coefficients with the results of estimates based on the vacuum saturation approximation (VSA). In Sec. VI D we will compare the present results with those from our fits to the OPAL data.

### A. Tests

We consider first the comparison of the experimental value of

$$I^{(\hat{w}_3)}_{{\rm ex},V}(s_0) + I^{(\hat{w}_3)}_{{\rm ex},A}(s_0) = \frac{m_\tau^2}{12\pi^2 |V_{ud}|^2 S_{\rm EW}} R_{V+A;ud}(s_0) \quad (6.1)$$

with the function obtained from the fit. In Fig. 11 we show this comparison, using the parameter values for $s_{\rm min} = 1.55$ GeV$^2$ from Table V. The fitted curves are in good agreement everywhere above $s_0 \approx 1.3\,{\rm GeV}^2$ ($s_0 \approx 1.5\,{\rm GeV}^2$) for the FOPT (CIPT) fits.[10] We include this test because (in rescaled form) it was originally advocated as an important confirmation of the analysis of Ref. [3]. One can see that our fits satisfy this test at least as well (see e.g. Fig. 73 of Ref. [3]). In other words, this test is not able to discriminate between the results of our analysis and those Refs. [1,3,4]. For more discussion on the comparison between our analysis and that of Refs. [1,3,4] we refer to Sec. VII.

As in Ref. [12], we may also consider the first and second Weinberg sum rules (WSRs) [23], as well as the Das-Guralnik-Mathur-Low-Young (DGMLY) sum rule for the pion electromagnetic mass splitting [24]. These sum rules can be written as

[10] We recall that even though correlations between different spectral moments are not included in the fit quality $\mathcal{Q}^2$, those between bins within one spectral moment are included, making these fits strongly correlated.

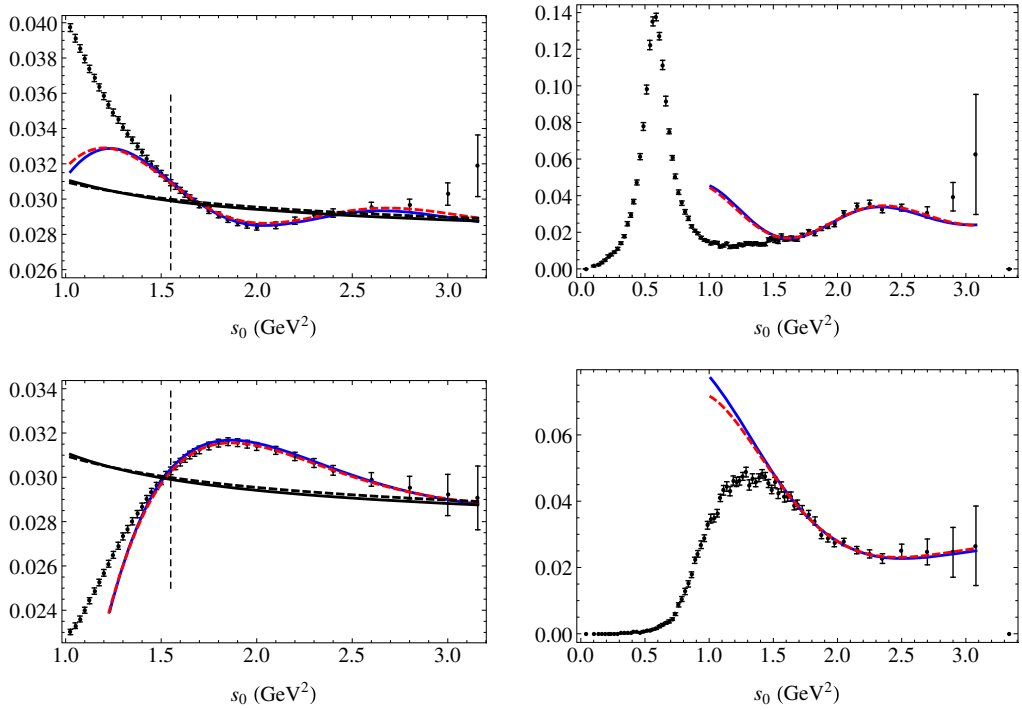


FIG. 10 (color online). (Left panels) Comparison of $I_{\rm ex}^{(\hat{w}_0)}(s_0)$ and $I_{\rm th}^{(\hat{w}_0)}(s_0)$ for the $s_{\rm min} = 1.55$ GeV$^2$ combined $V$ and $A$ channel fits of Table V ($V$ top, $A$ bottom). (Right panels) Comparison of the theoretical spectral function resulting from this fit with the experimental results ($V$ top, $A$ bottom). CIPT fits are shown in red (dashed) lines and FOPT in blue (solid) lines. The (much flatter) black curves on the left represent the OPE parts of the fits. The vertical dashed line indicates the location of $s_{\rm min}$.

$$\int_0^\infty ds(\rho_V^{(1+0)}(s) - \rho_A^{(1+0)}(s)) = \int_0^\infty ds(\rho_V^{(1)}(s) - \rho_A^{(1)}(s)) - 2f_\pi^2 = 0,$$
$$\int_0^\infty dss(\rho_V^{(1+0)}(s) - \rho_A^{(1+0)}(s)) = \int_0^\infty dss(\rho_V^{(1)}(s) - \rho_A^{(1)}(s)) - 2m_\pi^2 f_\pi^2 = 0,$$
$$\int_0^\infty dss\log(s/\mu^2)(\rho_V^{(1)}(s) - \rho_A^{(1)}(s)) = \frac{8\pi f_0^2}{3\alpha}(m_{\pi^\pm}^2 - m_{\pi^0}^2), \tag{6.2}$$

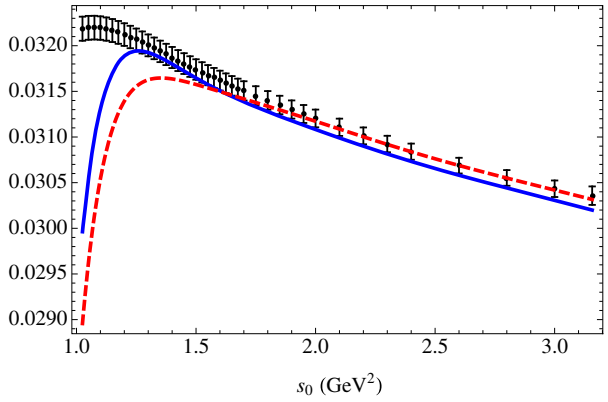


FIG. 11 (color online). The rescaled version of $R_{V+A;ud}(s_0)$ [the rhs of Eq. (6.1)] as a function of $s_0$. Theory curves from $s_{\rm min} = 1.55$ GeV$^2$ entries of Table V; CIPT (red, dashed line) and FOPT (blue, solid line).

where $f_0$ is the pion decay constant in the chiral limit, and $\alpha$ is the fine-structure constant. For the second WSR we assume that terms of order $m_i m_j$, $i, j = u, d$ can be neglected. Without this assumption, the integral is linearly divergent, forcing us to cut it off. If we cut off the integral at $s_0$, there would be an extra contribution proportional to $m_i m_j \alpha_s^2 s_0$ in this sum rule. This contribution is still very small at $s_0 = m_\tau^2$ (of order a few percent of the contribution $2m_\pi^2 f_\pi^2$), allowing us to assume that we are effectively in the chiral limit with regard to the second WSR. Even the term $2m_\pi^2 f_\pi^2$, while dominating the term proportional to $m_i m_j \alpha_s^2 s_0$, vanishes in the chiral limit, and itself turns out to be numerically negligible within errors. Also the DGMLY sum rule holds only in the chiral limit, and in that limit the integral on the left-hand side is independent of $\mu$ because of the second WSR.

In Fig. 12 we show the first integral in Eq. (6.2) as a function of the "switch" point $s_{\rm sw}$ below which we use the

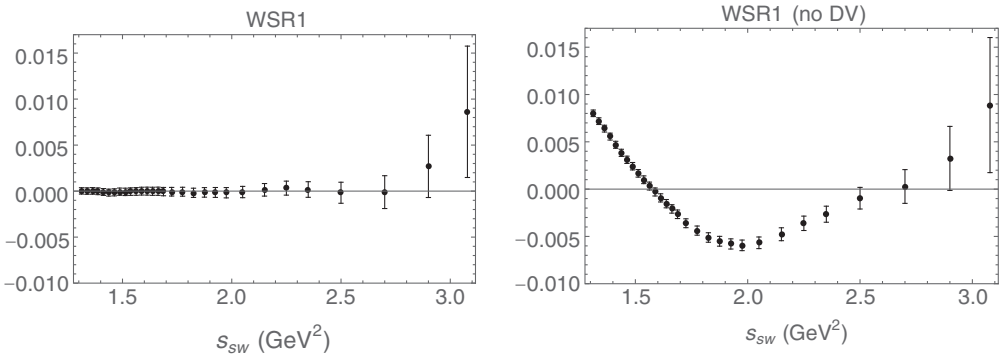


FIG. 12. The first Weinberg sum rule, with DVs (left panel) and without DVs (right panel), both in GeV$^2$. Data have been used for $s < s_{\rm sw}$, while the DV ansatz (2.10) with parameter values obtained from the $s_{\rm min} = 1.55$ GeV$^2$ fit has been used for $s > s_{\rm sw}$. The figures shown use CIPT fits.

experimental data, and above which we use the DV ansatz (2.10) with parameters from the CIPT fit with $s_{\rm min} = 1.55$ GeV$^2$ of Table V in order to evaluate the integral. Using parameter values from Table IV or FOPT fits leads to almost identical figures.[11] The figure on the left includes the contribution from Eq. (2.10), while the figure on the right omits such contributions. The latter is equivalent to the upper right panel of Fig. 8 in the first paper in Ref. [3]. Clearly, the first WSR is very well satisfied by our fits, but only if duality violations are taken into account. We do not show similar figures for the second WSR and the DGMLY sum rule, because our conclusions for these sum rules are very similar. Just as in Ref. [12,13], these sum rules are satisfied within errors, but only if duality violations are taken into account. In particular, within errors, one may assume that our representation of the spectral functions is in the chiral limit, for the purpose of these three sum rules.

### B. The strong coupling

The presence of duality violations forces us to make several assumptions in order to extract a value for $\alpha_s(m_\tau^2)$. These assumptions have been checked against the data, cf. Figs. 5 and 8–12. First, we need to assume that Eq. (2.10) provides a satisfactory description of duality violations for asymptotically large $s$. Second, we need to assume that $s \gtrsim 1.5$ GeV$^2$ is already in the asymptotic region. And, finally, if we wish to also use the axial data, we need to assume that this is true both in the $V$ and $A$ channels. As already discussed above, this would amount to the assumption that the upper shoulder of the $a_1$ resonance is already more or less in the asymptotic region. Using only the $V$-channel fits, we avoid having to make this latter assumption, and doing so we find, from the results quoted in Eq. (5.2),

$$\begin{aligned}\alpha_s(m_\tau^2) &= 0.296(10)(1)(2) = 0.296 \pm 0.010 \qquad (\overline{\rm MS}, n_f = 3, {\rm FOPT}),\\ &= 0.310(14)(1)(1) = 0.310 \pm 0.014 \qquad (\overline{\rm MS}, n_f = 3, {\rm CIPT}),\end{aligned} \tag{6.3}$$

where the first error is the statistical fit error already given in Eq. (5.2), while the second represents half the difference between the $s_{\rm min} = 1.55$ and $1.575$ GeV$^2$ results of Table III from which the average is derived. The third error represents the change induced by varying the estimated 6-loop $D = 0$ coefficient $c_{51} = 283$ [15] by the assumed 100% uncertainty about its central value, as in Refs. [12,13]. The error from this latter uncertainty would be about $\pm 0.004$ for both FOPT and CIPT if it were estimated from fits using only the moment with weight $\hat{w}_0$; this would raise both final errors by 0.001. We observe that the final errors we find are of the same order of magnitude as the difference between the FOPT and CIPT values of $\alpha_s(m_\tau^2)$. We also note that in all tables the value of $\alpha_s(m_\tau^2)$ is very stable as a function of $s_{\rm min}$ for all values of $s_{\rm min}$ included in these tables, except for possibly the lowest $s_{\rm min}$ shown.

Equation (6.3) constitutes our final result for $\alpha_s(m_\tau^2)$ from the revised ALEPH data. Converting these results into values for $\alpha_s$ at the $Z$ mass using the standard self-consistent combination of 4-loop running with 3-loop matching at the flavor thresholds [39], we find

$$\begin{aligned}\alpha_s(m_Z^2) &= 0.1155 \pm 0.0014 \qquad (\overline{\rm MS}, n_f = 5, {\rm FOPT}),\\ &= 0.1174 \pm 0.0019 \qquad (\overline{\rm MS}, n_f = 5, {\rm CIPT}).\end{aligned} \tag{6.4}$$

[11]The contribution from OPE terms to the spectral functions $\rho_{V,A}$ is suppressed by an extra power of $\alpha_s$, and small enough to be negligible [11,12].

### C. Nonperturbative quantities

As in Ref. [13], we would like to estimate the relative deviation of the aggregate dimension-6 condensates $C_{6,V/A}$ from the values given by the VSA. We express these condensates in terms of the VSA-violating parameters $\rho_1$ and $\rho_5$ by [7]

$$C_{6,V/A} = \frac{32}{81}\pi\alpha_s(m_\tau^2)\langle\bar{q}q\rangle^2\begin{pmatrix} 2\rho_1 - 9\rho_5 \\ 11\rho_1 \end{pmatrix}, \quad (6.5)$$

with VSA results for $C_{6,V/A}$ corresponding to $\rho_1 = \rho_5 = 1$. Using $\langle\bar{q}q(m_\tau^2)\rangle = (-272\ \text{MeV})^3$ [40], and the averages of the results for $C_{6,V}$ and $C_{6,A}$ from the $s_{\min} = 1.55$ and 1.575 GeV$^2$ fits of Table V, we find[12]

$$\begin{aligned} &\rho_1 = -4 \pm 4, \qquad \rho_5 = 5.9 \pm 0.9 \qquad (\text{FOPT}), \\ &\rho_1 = -2 \pm 3, \qquad \rho_5 = 5.9 \pm 0.8 \qquad (\text{CIPT}). \end{aligned} \quad (6.6)$$

While no conclusion can be drawn about the accuracy of the VSA for $\rho_1$, it is clear that the VSA is a poor approximation for $\rho_5$. The value for $\rho_5$ is consistent with the one we found from OPAL data in Ref. [13].

It is conventional to characterize the size of nonperturbative contributions to the ratio $R_{V+A;ud} = R_{V;ud} + R_{A;ud}$ of the total nonstrange hadronic decay width to the electron decay width, where $R_{V/A;ud}$ have been defined in Eq. (2.5), by the parametrization

$$R_{V+A;ud} = N_c S_{\text{EW}}|V_{ud}|^2(1 + \delta_P + \delta_{\text{NP}}), \quad (6.7)$$

where $\delta_P$ stands for the perturbative, and $\delta_{\text{NP}}$ for the nonperturbative contributions beyond the parton model. If one knows $\delta_{\text{NP}}$, the quantity $\delta_P$, and hence $\alpha_s(m_\tau^2)$, can be determined from the experimental value of $R_{V+A;ud}$. In such an approach, the error on $\alpha_s(m_\tau^2)$ is thus directly correlated with that on $\delta_{\text{NP}}$. As in Ref. [13], our fits give access to the values of $\delta_{\text{NP}}$, as well as those of $\delta^{(6)}$, $\delta^{(8)}$ and $\delta^{\text{DV}}$, the contributions to $\delta_{\text{NP}}$ from the $D = 6$ and $D = 8$ terms in the OPE as well as the DV term. From the $s_{\min} = 1.55$ GeV$^2$ fits of Table V, we find

$$\begin{aligned} &\delta^{(6)} = 0.058 \pm 0.026, \qquad \delta^{(8)} = -0.036 \pm 0.017, \\ &\delta_{\text{DV}} = -0.0016 \pm 0.0011 \qquad (\text{FOPT}), \\ &\delta^{(6)} = 0.040 \pm 0.024, \qquad \delta^{(8)} = -0.024 \pm 0.015, \\ &\delta_{\text{DV}} = -0.0009 \pm 0.0009 \qquad (\text{CIPT}). \end{aligned} \quad (6.8)$$

The FOPT and CIPT estimates for these quantities are consistent with each other. There is a strong correlation between $\delta^{(6)}$ and $\delta^{(8)}$, about $-0.97$ in the FOPT case.

The values for $\delta^{\text{NP}}$ derived from these results are

$$\begin{aligned} &\delta^{\text{NP}} = 0.020 \pm 0.009 \qquad (\text{FOPT}), \\ &\delta^{\text{NP}} = 0.016 \pm 0.010 \qquad (\text{CIPT}), \end{aligned} \quad (6.9)$$

which differ by 1.6 and $1.2\sigma$, respectively, from the values found using the OPAL data in Ref. [13]. With the value $R_{V+A;ud} = 3.475(11)$ quoted in Ref. [1], one finds $\delta_P \approx 0.18$, an order of magnitude larger than $\delta_{\text{NP}}$, indicating that $R_{V+A;ud}$ is a dominantly perturbative quantity. However, as in Ref. [13], we find an error on $\delta_{\text{NP}}$ much larger than that reported by standard analyses in the literature, almost an order of magnitude so, for example, when compared to Ref. [1]. The result is that the error on $\alpha_s(m_\tau^2)$ is underestimated in the standard analysis; for further discussion, we again refer to Sec. VII below.

### D. Comparison with the fits of Ref. [13] to OPAL data

A particularly interesting check is to look for consistency of the results from our fits to the ALEPH data with those we obtained by fitting the OPAL data in Ref. [13]. For the strong coupling, our results from OPAL data were

$$\begin{aligned} \alpha_s(m_\tau^2) &= 0.325 \pm 0.018 \qquad (\overline{\text{MS}}, n_f = 3, \text{FOPT}, \text{OPAL}, \text{Ref}[13]), \\ &= 0.347 \pm 0.025 \qquad (\overline{\text{MS}}, n_f = 3, \text{CIPT}, \text{OPAL}, \text{Ref}[13]). \end{aligned} \quad (6.10)$$

The values (6.3) we find from the ALEPH data are 1.4 and $1.3\sigma$, respectively, lower than the OPAL values, assuming that the errors on the ALEPH and OPAL values are independent. We also note that the fits in Ref. [13] were not entirely unambiguous; a choice about the preferred range for $\delta_V$ had to be made. The fact that the difference between our central ALEPH- and OPAL-based values, as well as that between our central CIPT- and FOPT-based results, is, in each case, comparable in size to the error obtained in any of these analyses supports the notion that any improvement in the precision with which $\alpha_s(m_\tau^2)$ can be determined from hadronic $\tau$ decays will require significant improvements to the data. Of course, this assumes that the fit ansatz employed is valid in the region of $s_0$ larger than about 1.5 GeV$^2$. We will return to this point in Sec. VII below, as well as in the Conclusion.

The coupling $\alpha_s(m_\tau^2)$ is, of course, not the only fit parameter. One may for instance compare the values of the OPE and DV parameters between Table III above and Table 4 of Ref. [13] for $s_{\min} \approx 1.5$ GeV$^2$, and conclude that

[12]We neglected the smaller errors on $\alpha_s$ and $\langle\bar{q}q\rangle$.

they agree between the ALEPH and OPAL fits within (sometimes fairly large) errors. However, comparing Table V above with Table 5 of Ref. [13], one observes that the OPE and DV parameters for the axial channel agree less well between the ALEPH and OPAL fits. This may be an indication that it is safer to restrict our fits to the vector channel. Results for $\alpha_s(m_\tau^2)$ are, nevertheless, found to be consistent between pure-$V$ and combined $V$ and $A$ fits, both in this article and in Ref. [13].

### E. Final results for the strong coupling from ALEPH and OPAL data

To conclude this section, we present our best values for the strong coupling at the $\tau$ mass extracted from the ALEPH and OPAL data for hadronic $\tau$ decays, and based on the assumptions that underlie our analysis. The FOPT and CIPT averages, weighted according to the errors in Eqs. (6.3) and (6.10), are

$$\begin{aligned}\alpha_s(m_\tau^2) &= 0.303 \pm 0.009 \quad (\overline{\rm MS}, n_f = 3, \text{FOPT, ALEPH and OPAL}),\\ &= 0.319 \pm 0.012 \quad (\overline{\rm MS}, n_f = 3, \text{CIPT, ALEPH and OPAL}).\end{aligned} \tag{6.11}$$

These convert to the values

$$\begin{aligned}\alpha_s(m_Z^2) &= 0.1165 \pm 0.0012 \quad (\overline{\rm MS}, n_f = 5, \text{FOPT, ALEPH and OPAL}),\\ &= 0.1185 \pm 0.0015 \quad (\overline{\rm MS}, n_f = 5, \text{CIPT, ALEPH and OPAL}).\end{aligned} \tag{6.12}$$

## VII. THE ANALYSIS OF REF. [1]

We now turn to a discussion of what we have referred to as the standard analysis, which was used in Refs. [1,3,4,8], and is based on Ref. [9]. We begin with a brief overview of what is done in this approach. One considers spectral moments with the weights

$$\begin{aligned}w_{k\ell}(x) &= (1-x)^2(1+2x)(1-x)^k x^\ell,\\ x &= s/s_0,\end{aligned} \tag{7.1}$$

choosing $(k,\ell) \in \{(0,0),(1,0),(1,1),(1,2),(1,3)\}$, and evaluating these moments at $s_0 = m_\tau^2$ only. Ignoring logarithms,[13] terms in the OPE contribute to these weights up to $D = 16$. The five $s_0 = m_\tau^2$ moment values are, of course, insufficient to determine the eight OPE parameters $\alpha_s(m_\tau^2)$, $\langle \frac{\alpha_s}{\pi} GG\rangle$, $C_6$, $C_8$, $C_{10}$, $C_{12}$, $C_{14}$ and $C_{16}$, so some truncation is necessary. The standard analysis approach to this problem is to assume the OPE coefficients $C_{D=2k}$ for $D > 8$ are small enough that they may all be safely neglected in all of the FESRs under consideration, despite numerical enhancements of their contributions via larger coefficients in some of the higher degree weights. Duality violations are, similarly, assumed to be small enough that $\Delta(s)$ in Eq. (2.8) can be ignored as well, at least for $s_0$ close to $m_\tau^2$. With these assumptions, the remaining OPE parameters $\alpha_s(m_\tau^2)$, $\langle \frac{\alpha_s}{\pi} GG\rangle$, $C_6$ and $C_8$ are fitted using the $s_0 = m_\tau^2$ values of the five $w_{k\ell}$ spectral moments noted above, for each of the channels $V$, $A$ and $V+A$. The central values and errors for $\alpha_s(m_\tau^2)$ are taken from the fits (FOPT and CIPT) to the $V+A$ channel, based on the VSA-motivated expectation of significant $D = 6$ cancellation and the hope of similar strong DV cancellations in the $V+A$ sum. However, as we have seen in Eq. (6.6), VSA is a rather poor approximation. Furthermore, the fact that the spectral function for the $V+A$ combination is flatter in the region between 2 and 3 GeV$^2$ than is the case for the $V$ or $A$ channels separately may mislead one into believing that DVs are already negligible at these scales for the $V+A$ combination. In actual fact, however, though somewhat reduced in the $V+A$ sum, DV oscillations are still evident in the ALEPH $V+A$ distribution. In addition, since we have a good representation of the individual $V$ and $A$ channels, we also have a good representation of their sum. The fact that our fits yield results for $\gamma_A$ significantly larger than those for $\gamma_V$ implies that the level of reduction of DV contributions in going from the separate $V$ and $A$ channels to the $V+A$ sum is accidental in the window between 2 and 3 GeV$^2$, and does not persist to higher $s$, where the stronger exponential damping in the $A$ channel would drive the result for the $V+A$ sum towards that for the $V$ channel alone.

These assumptions should be compared with those that have to be made in order to carry out the analysis presented in this article (as well as in the OPAL-based analyses of Refs. [12,13]). DVs are unambiguously present in the spectral functions, as can be seen, for example, in the relevant panels of Figs. 5, 8, 9 and 10. In the standard analysis, the hope is that the double or triple pinching of the weights in Eq. (7.1) is sufficient to allow DVs to be ignored altogether, and indeed, for example Fig. 8, shows that pinching significantly reduces the role of DV contributions, especially near $s_0 = m_\tau^2$. However, if, as in the standard analysis, one restricts one's attention to $s_0 = m_\tau^2$, and

[13]Which appear in subleading terms in $\alpha_s$ at each order in the OPE.

wishes to employ only weights which are at least doubly pinched, the number of OPE parameters to be fit will necessarily exceed the number of weights employed, making additional assumptions, such as the truncation in dimension of the OPE described above, unavoidable.[14] With the standard-analysis choice of the set of weights of Eq. (7.1), one finds that the OPE must be truncated at dimension $D = 8$ in order to leave at least one residual degree of freedom in the fits. In our analysis, in contrast, we choose not to ignore DVs *a priori*. This requires us to model their contribution to the spectral functions [as we did through Eq. (2.10)], and to use not just the single value $s_0 = m_\tau^2$, but rather a range of $s_0$ extending down from $m_\tau^2$. The one assumption we *do* have to make is that the ansatz (2.10) provides a sufficiently accurate description of DVs for values of $s_0$ between approximately 1.5 GeV$^2$ and $m_\tau^2$.

Clearly, whatever choice is made, it needs to be tested. For our analysis framework, we have presented detailed tests already above. In this section we consider primarily the standard analysis, most recently used in Ref. [1]. Our conclusion, from what follows below, is that the assumptions made in this framework do not hold up to quantitive scrutiny, and hence that the standard analysis approach should no longer be employed in future analyses.[15]

The results presented in Table 4 of Ref. [1] already indicate that there are problems with the standard analysis. Let us consider the values obtained for the gluon condensate, $\langle \frac{\alpha_s}{\pi} GG \rangle$, in the different channels, together with the $\chi^2$ value for each fit (recall that for each of these fits there is only one degree of freedom):

$$\begin{aligned} \left\langle \frac{\alpha_s}{\pi} GG \right\rangle &= (-0.5 \pm 0.3) \times 10^{-2}\ \text{GeV}^4, \quad \chi^2 = 0.43 \quad V, \\ &\quad (-3.4 \pm 0.4) \times 10^{-2}\ \text{GeV}^4, \qquad \chi^2 = 3.4 \quad A, \\ &\quad (-2.0 \pm 0.3) \times 10^{-2}\ \text{GeV}^4, \quad \chi^2 = 1.1 \quad V + A. \end{aligned} \tag{7.2}$$

The $\chi^2$ values correspond to $p$-values of 51%, 7% and 29%, respectively, indicating that all fits are acceptable. For these fits to be taken as meaningful, however, their results should satisfy known physical constraints. One such constraint is that there is only one effective gluon condensate, whose values should therefore come out the same in all of the $V$, $A$ and $V + A$ channels. This is rather far from the case for the results quoted in Eq. (7.2), where, for example, the $V$ and $V + A$ channel fit values differ very significantly. It is, moreover, problematic to accept the $V + A$ channel value and ignore the $V$ channel one when the $p$-value of the $V$-channel fit is, in fact, larger than that of the $V + A$ channel.

There can be several reasons for the inconsistencies in the results of Ref. [1]. One possibility is that some of the weights (7.1) have theoretical problems already in perturbation theory, as argued in Ref. [31]. Another possibility is that the assumptions underlying the standard analysis do not hold. Whatever the reason, the discrepant gluon condensate values point to a serious problem with the standard analysis framework.[16]

We now turn to quantitative tests of the OPE fit results reported in Ref. [1]. We focus on the $V + A$ channel, where DVs and $D > 4$ OPE contributions were expected to play a reduced role, and on the CIPT $D = 0$ treatment, since this is the only case for which the OPE fit parameter values are quoted in Ref. [1]. The tests consist of comparing the weighted OPE and spectral integrals for the weights $w_{k\ell}$ employed in the analysis of Ref. [1], not just at $s_0 = m_\tau^2$, but over an interval of $s_0$ extending below $m_\tau^2$. If the assumptions made about $D > 8$ OPE and DV contributions being negligible are valid at $s_0 = m_\tau^2$ they should also be valid in some interval below this point. A good match between the weighted spectral integrals and the corresponding OPE integrals, evaluated using the results for the OPE parameters quoted in Ref. [1], should thus be found over an interval of $s_0$. If, on the other hand, these assumptions are not valid, then the fit parameter values will contain contaminations from DV contributions and/or contributions with higher $D$, both of which scale differently with $s_0$ than do the $D = 0$, 4, 6 and 8 contributions appearing in the truncated OPE form. Such contamination will show up as a disagreement between the $s_0$ dependence of the fitted OPE representations and the experimental spectral integrals.

It is worth expanding somewhat on this latter point since the agreement of the OPE and spectral integrals at $s_0 = m_\tau^2$ for the weights $w_{k\ell}$ employed in the standard analysis is sometimes mistakenly interpreted as suggesting the validity of the assumptions underlying the standard analysis at $s_0 = m_\tau^2$. However, while the agreement is certainly a necessary condition for the validity of these assumptions, it is not in general a sufficient one. This caution is particularly relevant since four parameters are being fit using only five data points, making it relatively easy for the effects of neglected, but in fact non-negligible, higher-$D$ and/or DV contributions to be absorbed, *at a fixed* $s_0$, into the values of the four fitted lower-$D$ parameters. That this is a realistic possibility is demonstrated by the alternate set of OPE fit parameters obtained in the analysis of Ref. [10], which neglected DV contributions, but not OPE

[14]For a detailed discussion of this point, see Ref. [12].

[15]We point out that the inadequacy of the standard analysis framework was already demonstrated in Refs. [10–13], but it appears important to reemphasize this point in view of the continued use of this framework in the literature, in particular in the updated analysis of Ref. [1].

[16]This problem already existed in earlier ALEPH analyses [3,4], but in principle it might have been due to the problem with the data itself. Note that OPAL enforced equality of the gluon condensate between various channels, and were able to obtain reasonable fits as judged by the $\chi^2$, possibly because of the larger data errors.

contributions with $D > 8$. The results of this fit, including nonzero $C_D$ with $D > 8$ and an $\alpha_s(m_\tau^2)$ significantly different from that obtained via the standard analysis of the same data [4], produced equally good agreement between the $s_0 = m_\tau^2$ OPE and spectral integral results for all the $w_{k\ell}$ employed in the standard analysis fit of Ref. [4], conclusively demonstrating that this agreement does not establish the validity of the standard analysis assumptions. So long as one works at fixed $s_0 = m_\tau^2$, there is no way to determine whether the results of the standard analysis are, in fact, contaminated by neglected higher-$D$ OPE and/or DV effects or not. One may, however, take advantage of the fact that different contributions to the theory sides of the various FESRs scale differently with $s_0$, with integrated DV contributions oscillatory in $s_0$ and integrated $D = 2k$ OPE contributions scaling as $1/s_0^k$. If the $D = 0$, 4, 6 and 8 parameters obtained from the fixed-$s_0 = m_\tau^2$ standard analysis fit have, in fact, absorbed the effects of $D > 8$ and/or DV contributions, the fact that the nominal lower-$D$ $s_0$ scaling does not properly match that of the higher-$D$ and/or DV contaminations will be exposed when one considers the same FESR, with the same standard analysis OPE fit parameter values, at lower $s_0$. A breakdown of the standard analysis assumptions will thus be demonstrated by a failure of the agreement of the OPE and spectral integrals observed at $s_0 = m_\tau^2$ to persist over a range of $s_0$ below $m_\tau^2$. Such $s_0$-dependence tests represent important self-consistency checks for all FESR analyses.

Before carrying out these self-consistency tests on the results of the standard analysis, it is useful to make explicit the relative roles of the various different $D$ contributions entering the $s_0 = m_\tau^2$ results for the $w_{k\ell}$-weighted OPE integrals employed in the $V + A$ CIPT fit of Ref. [1]. For the $D = 0$ contributions, it is important to remember that the leading 1-loop contribution is independent of both $s_0$ and $\alpha_s$. It is thus the difference of the full $D = 0$ contribution and this leading term which determines the $\alpha_s$ dependence of the $D = 0$ contributions, and which is relevant to the determination of $\alpha_s(m_\tau^2)$. Table VI shows the $s_0 = m_\tau^2$ results for (i) the $\alpha_s$-dependent $D = 0$ contributions and (ii) the $D = 4$, 6 and 8 contributions corresponding to the CIPT fit results of Table 4 of Ref. [1], for each of the $w_{k\ell}$ employed in that analysis. The sum of the $D = 6$ and 8 contributions, which is ∼1%–2% of the $\alpha_s$-dependent $D = 0$ contribution for $w_{00}$ and $w_{10}$, is, in contrast, ∼10%–25% of the corresponding $D = 0$ contributions for the $w_{11}$, $w_{12}$ and $w_{13}$ cases. Furthermore, for $w_{11}$, the $D = 4$ contribution is essentially the same size as the $\alpha_s$-dependent $D = 0$ one.

TABLE VI. The $D = 4$, 6 and 8 and $\alpha_s$-dependent $D = 0$ contributions to the $s_0 = m_\tau^2$, $V + A$, $w_{k\ell}$ moments corresponding to the $V + A$ OPE fit parameter results of Table 4 of Ref. [1].

| $(k,\ell)$ | $\alpha_s$-dependent $D = 0$ | $D = 4$ | $D = 6$ | $D = 8$ |
|---|---|---|---|---|
| (0,0) | 0.005173 | −0.000008 | −0.000117 | 0.000033 |
| (1,0) | 0.004399 | −0.000361 | −0.000117 | 0.000082 |
| (1,1) | 0.000365 | 0.000350 | −0.000039 | −0.000049 |
| (1,2) | 0.000208 | 0.000002 | 0.000039 | −0.000016 |
| (1,3) | 0.000081 | 0.000000 | 0.000000 | 0.000016 |

It is clear from these observations that it is the $w_{11}$, $w_{12}$ and $w_{13}$ moments which dominate the determinations of the $D = 4, 6$ and 8 OPE parameters in the analysis of Ref. [1]. Bearing in mind the very slow variation with $s_0$ of the $D = 0$ contributions to the dimensionless OPE integrals and the $1/s_0^k$ scaling of the $D = 2k$ contributions, it is, moreover, clear that the relative roles of the nonperturbative contributions will grow significantly relative to the $\alpha_s$-dependent $D = 0$ ones as $s_0$ is decreased. Studying the $s_0$ dependence of the match of the OPE to the corresponding spectral integrals for the $w_{11}$, $w_{12}$ and $w_{13}$ spectral weights thus provides a particularly powerful test of the reliability of the values for the $D = 4, 6$ and 8 parameters obtained in the fits of Ref. [1].

The results of these tests are shown in Fig. 13. It is clear that the $s_0$ dependence of the experimental spectral integrals and fitted OPE integrals is very different, demonstrating conclusively the unreliability of the $D = 4, 6$ and 8 fit parameter values obtained in Ref. [1]. Changes in the values of the $D = 6$ and 8 parameters, which enter the $w_{00}$ FESR, would of course also force a change in the $\alpha_s(m_\tau^2)$ required to produce a match between the $s_0 = m_\tau^2$ $w_{00}$-weighted OPE and spectral integrals.

It is worth expanding somewhat on these observations for the $w_{13}$ case, where the source of the problem with the fit of Ref. [1] becomes particularly obvious. Because of the $x^3$ factor present in $w_{13}(x)$, the $D = 2$ and 4 contributions to the OPE part are completely negligible numerically, leaving the standard-analysis version of the $w_{13}$-weighted OPE integral entirely determined by the parameters $\alpha_s(m_\tau^2)$ and $C_{8,V+A}$. With the results and errors for these quantities from Tables 4 and 5 of Ref. [1], one finds that, as $s_0$ is decreased from $m_\tau^2$ to e.g. 2 GeV$^2$, the $\alpha_s$-dependent $D = 0$ contribution *decreases* by 0.000001(0), while the $D = 8$ contribution *increases* by 0.000086(20). This is to be compared to the increase in the corresponding spectral integral, which is 0.000028(8). Evidently the disagreement between the $w_{13}$-weighted OPE and spectral integral results seen in Fig. 13 results from a problem with the fit value for $C_{8,V+A}$. Trying to fix the problem with the $w_{13}$ FESR through a change in $C_{8,V+A}$ alone turns out to exacerbate the problem with the $w_{12}$ FESR. Working backward, one finds that attempting to change $C_{4,V+A}$, $C_{6,V+A}$ and $C_{8,V+A}$ so as to improve the match between the $s_0$ dependences of the OPE and spectral integrals for the $w_{11}$, $w_{12}$ and $w_{13}$ FESRs without any change in $\alpha_s(m_\tau^2)$ produces changes in the $D \geq 4$ contributions to the $w_{10}$ and $w_{00}$ FESRs that can only be compensated for by a decrease in $\alpha_s(m_\tau^2)$. The problem of the discrepancies between the $s_0$ dependences

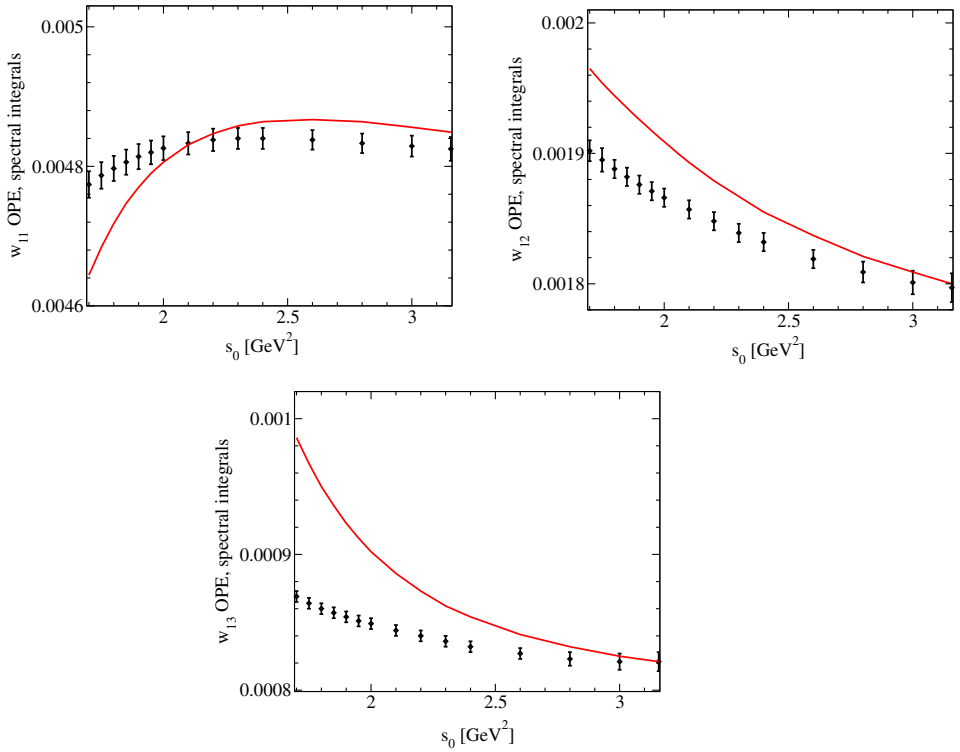


FIG. 13 (color online). Comparisons of the $s_0$ dependence of the $w_{k\ell} = w_{11}$, $w_{12}$ and $w_{13}$ $V+A$ spectral integrals to that of the corresponding OPE integrals evaluated employing as input the results of the CIPT fit for the OPE parameters from Table 4 of Ref. [1].

of the OPE and spectral integrals in the $w_{11}$, $w_{12}$ and $w_{13}$ FESR parts of the standard analysis can thus not be resolved simply through shifts in $C_{4,V+A}$, $C_{6,V+A}$ and $C_{6,V+A}$ which leave the target of the analysis, namely the output $\alpha_s(m_\tau^2)$ value, unchanged.

A natural question, given the discussion above, is whether our approach produces a better match between experiment and theory for the higher spectral weights. The answer, as we will see below, is yes. Before embarking on this investigation, however, it is important to emphasize the nonoptimal nature of the FESRs with weights $w_{10}$, $w_{11}$, $w_{12}$ and $w_{13}$. First, all of these weights contain a term linear in the variable $x$, a fact which, according to the arguments of Ref. [31], should make standard methods of estimating the uncertainty associated with truncating the integrated perturbative series for these weights much less reliable than is the case for the weights employed in our analysis. Second, the values of the $C_D$ with $D > 8$ obtained from the fits reported in Ref. [10] were found to produce very strong cancellations amongst higher-$D$ OPE contributions when employed in the higher $(k,\ell)$ $w_{k\ell}$ FESRs, making these FESRs particularly sensitive to any shortcomings in the treatment of higher-$D$ OPE contributions, as well as a poor choice for use in attempting to fit the values of $C_D$ with $D > 8$. The strong cancellation amongst higher-$D$ OPE contributions for the higher-$(k,\ell)$ $w_{k\ell}$ moments turns out to be also a feature of the results of our extended analysis below, and hence not attributable to the neglect of DV contributions in Ref. [10]. Because of these strong cancellations, the use of the higher-$(k,\ell)$ $w_{k\ell}$ should be avoided in future analyses, and we consider them below only for the sake of comparison with the results of the analysis of Ref. [1]. In making this comparison, we will focus on the CIPT resummation of perturbation theory, with the CIPT version of the standard analysis being the only one for which quantitative fit results are reported in Ref. [1].

To evaluate the OPE contributions to the $w_{10}$, $w_{11}$, $w_{12}$ and $w_{13}$ FESRs requires knowledge of five new quantities, $C_{4,V+A}$, $C_{10,V+A}$, $C_{12,V+A}$, $C_{14,V+A}$ and $C_{16,V+A}$, in addition to the OPE and DV parameters already obtained in our analysis. We estimate these using the $w(s) = (s/s_0)^{k-1}$ versions of the FESR Eq. (2.9), neglecting, as before, subleading contributions at each order $D > 2$ in the OPE. This yields, for $D = 2k > 2$,

$$(-1)^{k+1}C_{2k,V+A} = 2f_\pi^2 m_\pi^{2(k-1)} + \int_0^{s_0} ds s^{k-1}\rho_{V+A}^{(1)}(s) + \int_{s_0}^{\infty} ds s^{k-1}\rho_{V+A}^{\rm DV}(s) + \frac{1}{2\pi i}\oint_{|z|=s_0} dz z^{k-1}\Pi_{V+A}^{\rm PT}(z), \qquad (7.3)$$

where $\Pi^{\rm PT}$ is the perturbative contribution to $\Pi(z)$, corresponding to the $D = 0$ term in Eq. (2.6). The choices

$k = 2, \cdots, 8$ yield $C_4, \cdots, C_{16}$, respectively. With $\alpha_s(m_\tau^2)$ and the $V$ and $A$ channel DV parameters from the $s_{\min} = 1.55$ GeV$^2$ combined $V$ and $A$ CIPT fit of Table V, we find, for the central values,

$$\begin{aligned} C_{4,V+A} &= 0.00268 \text{ GeV}^4, \\ C_{6,V+A} &= -0.0125 \text{ GeV}^6, \\ C_{8,V+A} &= 0.0349 \text{ GeV}^8, \\ C_{10,V+A} &= -0.0832 \text{ GeV}^{10}, \\ C_{12,V+A} &= 0.161 \text{ GeV}^{12}, \\ C_{14,V+A} &= -0.191 \text{ GeV}^{14}, \\ C_{16,V+A} &= -0.233 \text{ GeV}^{16}. \end{aligned} \tag{7.4}$$

For $C_{6,V+A}$ and $C_{8,V+A}$ the agreement with the values in Table V is excellent. With such values of the $C_D$, $D > 8$ contributions are far from negligible compared to the $D = 6$ and 8 ones for the $w_{k\ell}$ spectral weights with degree higher than three; the maximum scale, $m_\tau^2$, accessible in hadronic $\tau$ decays is not, it turns out, high enough to ensure that the OPE series is rapidly converging in dimension.

The theory parts $I_{\rm th}^{(w_{k\ell})}(s_0)$ of the $w_{10}$, $w_{11}$, $w_{12}$ and $w_{13}$ FESRs produced by the results of Eq. (7.4) and Table V are compared to the corresponding spectral integrals in Fig. 14 as a function of $s_0$. The agreement is obviously excellent, and far superior to that obtained from the standard analysis of Ref. [1]. This excellent agreement, over the whole range of $s_0$ shown, is completely destroyed if one removes the $D > 8$ contributions from the theory sides of the $w_{10}$, $w_{11}$, $w_{12}$ and $w_{13}$ FESRs. We emphasize again that the aim here is not a reliable determination of the OPE coefficients $C_{4-16}$, but a proof of existence of a set of values which, combined with our values for $\alpha_s(m_\tau^2)$ and the DV parameters, give an excellent representation of the $s_0$ dependence of the moments with the weights $w_{10}$, $w_{11}$, $w_{12}$ and $w_{13}$ (in addition, of course, to the weights included in our fits, in particular $w_{00} = \hat{w}_3$).

The problems demonstrated above with the standard analysis results of Ref. [1] could be a consequence of the neglect of non-negligible DVs, the breakdown of the assumption that $D > 8$ OPE contributions are negligible for all of the $w_{k\ell}$ employed or both. In an attempt to clarify the situation, it is useful to consider a fit in which the potentially dangerous assumption about $D > 8$ OPE contributions is avoided. As an example, we consider a fit to the doubly pinched $\hat{w}_3 = w_{00}$ FESR in the $V + A$ channel ignoring DV contributions. Since the weight is doubly pinched, one expects DV contributions to be significantly suppressed, though the actual amount of suppression is not clear *a priori*. Since the OPE integrals still depend on three parameters, $\alpha_s(m_\tau^2)$, $C_{6,V+A}$ and $C_{8,V+A}$, it is, of course, necessary to consider the fit over a range of $s_0$. To be

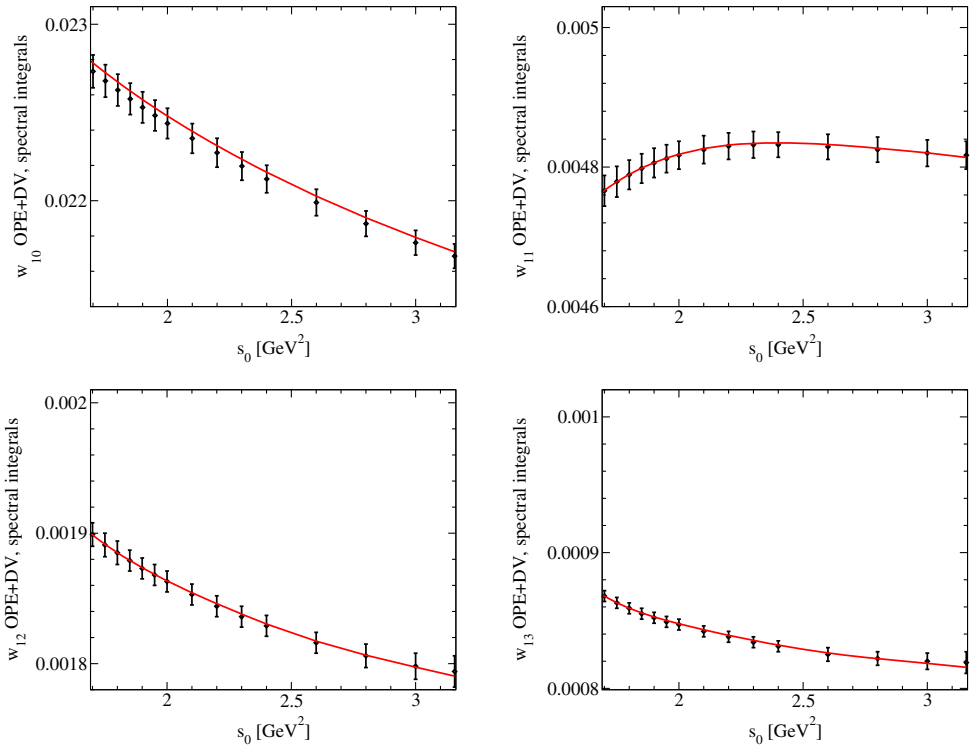


FIG. 14 (color online). Comparison of $I_{\rm th}^{(w_{k\ell})}(s_0)$ [cf. Eq. (2.9)] for $w_{k\ell} = w_{10}$, $w_{11}$, $w_{12}$ and $w_{13}$ with $I_{\rm ex}^{(w_{k\ell})}(s_0)$ for the $V + A$ channel using the results of the $s_{\min} = 1.55$ GeV$^2$, combined $V$ and $A$ CIPT fit of Table V and Eq. (7.4). (Top left panel) The $w_{10}$ case. (Top right panel) The $w_{11}$ case. (Bottom left panel) The $w_{12}$ case. (Bottom right panel) The $w_{13}$ case.

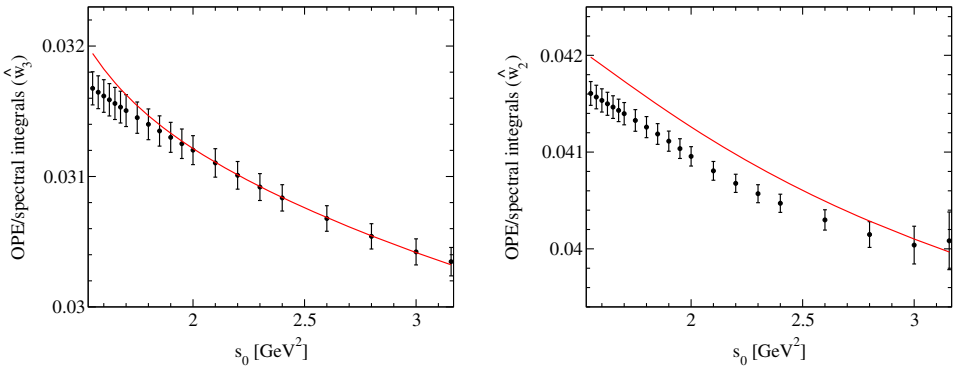


FIG. 15 (color online). Comparison of the $\hat{w}_3 = w_{00}$–weighted spectral integrals (left panel) and $\hat{w}_2$-weighted spectral integrals (right panel) with the corresponding OPE integrals evaluated using the results of the no-DV fit given in Eq. (7.5).

specific, we focus on fits employing the FOPT resummation of perturbation theory. This exercise results in apparently perfectly acceptable fits, with $p$-values 10% and higher for $s_{\min} \geq 1.95$ GeV$^2$. The fit quality drops dramatically as $s_0$ is lowered beyond this point, with $p$-values already at the 0.2% level for $s_{\min} = 1.90$ GeV$^2$. The highest $p$-value, 57%, occurs for $s_{\min} = 2.2$ GeV$^2$, and corresponds to

$$\begin{aligned} \alpha_s(m_\tau^2) &= 0.330 \pm 0.006, \\ C_{6,V+A} &= 0.0070 \pm 0.0022 \text{ GeV}^6, \\ C_{8,V+A} &= -0.0088 \pm 0.0042 \text{ GeV}^8. \end{aligned} \tag{7.5}$$

The quality of the resulting match between the fitted OPE and spectral integrals for $s_{\min} = 2.2$ GeV$^2$, shown in the left panel of Fig. 15, is excellent. Despite this good quality match, the results of Eq. (7.5) are incomplete, in the sense that, in addition to the fit error induced by the covariances of the $V + A$ spectral data, there is an unspecified (and hence unquantified) systematic error associated with the neglect of DV contributions in the fit. Since the DV contribution to the FESR (2.9) involves the weighted integral of the DV component of the spectral function in the interval $s \geq s_0$, neglecting this systematic error would be reasonable if the $V + A$ spectral distribution showed no signs of DVs in the region $s > 2.2$ GeV$^2$. This is, however, rather far from being the case, making the absence of an estimate for the residual systematic error associated with neglecting DV contributions problematic. One internally consistent way to test whether DV contributions are sufficiently small to be neglected for the $\hat{w}_3$ FESR is to demonstrate that they are already small for the singly pinched $\hat{w}_2$ FESR. Whether or not this is the case can be investigated by comparing the $\hat{w}_2$-weighted OPE and spectral integrals, in the same $s_0$ range, using parameters obtained from the no-DV fit to $\hat{w}_3$, Eq. (7.5). The results of this test are shown in Fig. 15 (right panel). The agreement between the OPE and spectral integrals is clearly not good, indicating the presence of significant DV contributions in the $\hat{w}_2$ FESR. This, together with the rapid deterioration of the $\hat{w}_3$ no-DV fit quality for $s_{\min} \leq 1.95$ GeV$^2$, suggests that neglecting DV contributions to the $\hat{w}_3$ FESR is also dangerous.

The hope underlying existing FESR analyses which ignore DV effects is that the double pinching of the weight $w_{00} = \hat{w}_3$ is sufficient to make the residual DV contributions very small. While the arguments above make this possibility unlikely, it is still logically possible that, although DVs cannot be ignored in the singly pinched $\hat{w}_2$ FESR, they can be ignored in the doubly pinched $\hat{w}_3$ FESR. Let us therefore consider again the FOPT version of the $\hat{w}_3$ FESR in the $V + A$ channel, but now, rather than ignoring DVs, taking as external input the results for the DV parameters from the $s_{\min} = 1.55$ GeV$^2$ FOPT fit of Table V and fitting the remaining OPE parameters, $\alpha_s(m_\tau^2)$, $C_{6,V+A}$ and $C_{8,V+A}$, to the $\hat{w}_3$-weighted spectral integral in the $V + A$ channel in the presence of this estimate of the DV contributions. The results of this exercise, which are to be compared with Eq. (7.5), are

$$\begin{aligned} \alpha_s(m_\tau^2) &= 0.301 \pm 0.006 \pm 0.009, \\ C_{6,V+A} &= -0.0127 \pm 0.0020 \pm 0.0066 \text{ GeV}^6, \\ C_{8,V+A} &= 0.0399 \pm 0.0040 \pm 0.021 \text{ GeV}^8, \end{aligned} \tag{7.6}$$

where the first error is statistical and the second is that induced by the correlated uncertainties of the external input DV parameters. The inclusion of the DV contributions induces a significant decrease in the value of $\alpha_s(m_\tau^2)$ and significant changes in the results for $C_{6,V+A}$ and $C_{8,V+A}$ (including changes in sign for both) as compared to the no-DV fit results of Eq. (7.5). The fit parameters are all changed in the direction of the results of the more detailed combined $V$ and $A$ fits discussed in Sec. V. This exercise clearly demonstrates that the effects of DVs on the parameters obtained from the $V + A$ $\hat{w}_3$ FESR analysis are much larger than the nominal errors obtained on those parameters from the no-DV fit. This provides a further indication of the necessity of modeling DV effects in

analyses attempting to extract $\alpha_s(m_\tau^2)$ from hadronic $\tau$-decay data.

## VIII. CONCLUSION

In this article, we reanalyzed the recently revised ALEPH data [1] for nonstrange hadronic $\tau$ decays, with as primary goal the extraction of the strong coupling $\alpha_s$ at the scale $m_\tau$. The rather low value of $m_\tau$ raises the question of to what extent the determination of a perturbative quantity like $\alpha_s$ in such an analysis might be "contaminated" by nonperturbative effects. Our specific aim was to take all known nonperturbative effects into account and arrive at a realistic estimate of the systematic error on the value of $\alpha_s$ extracted using hadronic $\tau$ data. This is important for three reasons. First, the value of $\alpha_s$ from $\tau$ decays, evolved to the $Z$ mass, has long been claimed to be one of the most precise values available. Second, because the $\tau$ mass is so much smaller than other scales at which the strong coupling has been determined, $\alpha_s(m_\tau^2)$ provides a powerful test of the QCD running of the strong coupling, with the corresponding $\beta$ function known to 4-loop order. Finally, there continues to be some tension between the values of the $n_f = 5$ coupling $\alpha_s(M_Z^2)$ obtained from different sources. Lattice determinations involving analyses of small-size Wilson loops [41,42], $c\bar{c}$ pseudoscalar correlators [43], the relevant combination of ghost and gluon two-point functions [44,45], and employing the Schrödinger functional scheme [46], for example, yield values, 0.1183(8) [41], 0.1192(11) [42], 0.1186(5) [43], 0.1196(11) [45], and 0.1205(20) [46], compatible both amongst one another and with the central value of the global electroweak fit result, $\alpha_s(M_Z^2) = 0.1196(30)$ [47]. Lower values, however, have been obtained in a number of other analyses, e.g., 0.1174(12) from lattice analyses of $f_\pi/\Lambda_{\rm QCD}$ [48], 0.1166(12) from an analysis of the static quark energy [49], 0.1118(17) from the recently revised JLQCD lattice determination from current-current two-point functions [50], and values in the range 0.1130–0.1160 from analyses of DIS data and shape observables in $e^+e^-$ [51].

We have employed our analysis method previously [12,13], using the OPAL data [8], but the revised ALEPH data have significantly smaller errors, and thus provide a more stringent test of our analysis method.

The fact that at such low scales nonperturbative effects are not negligible has of course been long known, and has been taken into account in the analysis of hadronic $\tau$ decays through the inclusion of higher-dimension condensate terms in the OPE. However, the experimental data are provided in the form of spectral functions, i.e., as functions of $s = q^2$ with $q$ denoting momentum in Minkowski space. Such values of $q^2$, viewed as a complex variable, are outside the domain of validity of the OPE. While this is well known, it can also easily be inferred from the form of the vector spectral function in Fig. 4, which clearly shows oscillations that cannot be represented by the OPE. These oscillations lead unavoidably to the conclusion that violations of quark-hadron duality are, in general, significant at the scales accessible through experimental hadronic $\tau$-decay data.

It follows that in order to investigate the effect of duality violations on the extraction of $\alpha_s$ from $\tau$-decay data, they need to be taken into account. Unfortunately, a model is needed in order to parametrize the oscillations in the spectral functions, and this modeling necessitates making some assumptions on which to base the analysis. This is, however, true for any such analysis: the assumption that duality violations can be ignored in a given analysis amounts to assuming a model as well; in terms of the ansatz (2.10) it corresponds to taking the parameters $\delta_{V,A}$ to $\infty$. We have, instead, assumed that this ansatz (with finite $\delta$) provides a reasonable model of the resonance features present in the spectral functions for values of $s$ in some region below $m_\tau^2$ in which perturbation theory is still meaningful.[17] As much as our aim is to find the most accurate value of $\alpha_s(m_\tau^2)$ possible given the data, an equally important goal was to test the validity of our approach, with the increased precision of the ALEPH data as compared to the OPAL data being particularly useful in this regard. This increased precision is, moreover, found to produce unique fit minima in the HROTHGAR studies of the multidimensional fit parameter space, improving the situation found for the corresponding fits to the OPAL data, and confirming that the precision of the ALEPH data is more than good enough to support fits incorporating an explicit representation of DV contributions.

Despite the recent resurgence of interest in this problem, triggered by the completion of the 5-loop calculation of the Adler function in Ref. [14], very few investigations have carried out a complete analysis starting from the data. In essence, only two methods have been proposed through which to investigate nonperturbative effects, with the first being the method based on Refs. [7,9], which was employed by Refs. [1,3,4,8], and the second being the method we employed in this article, applying and extending ideas proposed in earlier work [10,12,13,31]. In the absence of a detailed theoretical understanding of duality violations, it is important to test for the self-consistency of either analysis method using the data employed in the analysis.

In Sec. VII we demonstrated that the first method, used in Ref. [1], does not pass such tests. Indications supporting this conclusion have been published in earlier work, but now that the revised data are available, and in view of our critique in Sec. VII, we conclude that this method suffers from numerically significant systematic uncertainties not quantifiable within the analysis framework employed in Ref. [1], and hence must be discarded. The second method, employed in this article, does a much better job in fully describing the data, as we have shown in great detail in Secs. V, VI and VII above. However, there are some signs that also the limits of this method may be in view. Fit

[17] Up to the order considered [14].

qualities are typically larger than in the case of our analysis of the OPAL data [13], and a comparison of results based on ALEPH and OPAL data also shows some tension, even though errors are too large to say anything more conclusive. While these tensions may be caused by imperfections in the data (for instance slight discrepancies in the spectral function data visible in Fig. 4), it is by no means excluded that they point to shortcomings of the theory description as well.

We briefly reviewed, in Sec. II, why we consider the DV parametrization in Eq. (2.10) a physically sensible one. However, it remains relevant to test this form more quantitatively using experimental data. In this regard, we would like to stress that the exercise involving the $x^N$ FESRs leading to the results of Eq. (7.4) represents a highly nontrivial test of this type. This follows from the fact that DV contributions to the $x^N$ FESRs are generally not small, and oscillate with $s_0$. The $D = 0$ OPE and DV contributions to the theory side of the $x^N$ FESR for each $N$ are, in this exercise, fixed by the results of the earlier fits involving the ansatz (2.10), leaving only a $D = 2N + 2$ OPE contribution controlled by $C_{2N+2}$ to complete the theory side of the FESR. The different $x^N$ considered provide very different weightings on the interval from $s_0$ to $\infty$, and the different $s_0$ considered represent integration over different portions of the oscillations in the experimentally accessible region. Therefore, a problem with the DV ansatz would be expected to show up as an inability to successfully fit, with the single parameter $C_{2N+2}$, the $s_0$-dependent difference between the experimental spectral integrals and the sum of the previously fixed $D = 0$ OPE and DV theory integral contributions. In fact, as we have seen, a set of $C_{2N+2}$ exist which produce excellent matches to the experimental spectral integrals over a sizeable range of $s_0$ for all $N$ ($N = 1, \cdots, 7$) required to generate the results, shown in Fig. 14, for the weights $w_{k\ell}$ employed in Ref. [1]. The fact that the form (2.10) conforms to the qualitative features expected of the contribution representing the residual error of an asymptotic series, and the success of the detailed self-consistency tests just described, confirms that the ansatz (2.10) provides a good representation of DV effects in the channels of interest. Possible residual inaccuracies in this representation should, in any case, not be turned into an argument to not include DVs at all, since that strategy would lead to the presence of unquantifiable systematic errors which use of our ansatz strongly indicates are unlikely to be small.

It is interesting to compare the values of $\alpha_s(m_\tau^2)$ from the various analyses. First, the half differences between our ALEPH- and OPAL-based values are 0.015 (FOPT) and 0.019 (CIPT), while the average (between FOPT and CIPT) fit errors is about 0.012 for fits to ALEPH data [cf. Eq. (6.3)], and about double that for fits to OPAL data. Finally, the difference between the FOPT and CIPT values is 0.014 for the ALEPH-based values, and 0.022 for the OPAL-based values. These differences and errors are all comparable in size, and it appears reasonable to conclude that they reflect both the data and theory limitations on the accuracy with which $\alpha_s(m_\tau^2)$ can be obtained from analyses of hadronic $\tau$ decay, at least at present. We do not believe that it is meaningful to condense these results in the form of one central value and one aggregate error for $\alpha_s(m_\tau^2)$. Clearly, our ALEPH-based values are not in agreement with the value obtained in Ref. [1], despite using the same data. Averaging the values of Eq. (6.3) and adding half the difference between the two values as an error estimate for the CIPT/FOPT perturbative uncertainty, we would find a value $\alpha_s(m_\tau^2) = 0.303 \pm 0.014$, to be compared with the value $0.332 \pm 0.012$ quoted in Ref. [1]. It should be emphasized again that the error in the latter value does not include a component accounting for the systematic problems identified in Sec. VII.

One may ask whether one can do better. First, it would be interesting to apply our analysis method to data with better statistics, and such data are in principle available from the *BABAR* and Belle experiments. Such data would allow us to scrutinize our theoretical understanding in more detail and would, as can be seen from Fig. 4, be especially useful in the upper part of the spectrum. However, to date the analyses required to produce inclusive hadronic spectral functions from these data are not complete, and thus such an investigation must be postponed until they become available. Second, it would be nice to develop a deeper insight into the theory itself, or, lacking that, to develop new tools for testing any given model for duality violations. A recent idea in this direction based on functional analysis can be found in Ref. [52]. Finally, we note that the difference between the results for $\alpha_s(m_\tau^2)$ obtained using the FOPT and CIPT resummation schemes represents, at present, an important limitation on the accuracy with which $\alpha_s$ can be obtained at a scale as low as $m_\tau^2$; further progress will require an improved understanding of this issue.

## ACKNOWLEDGMENTS

We would like to thank Matthias Jamin for useful discussions, and Andy Mahdavi for the generous help with HROTHGAR. M. G. thanks IFAE and the Department of Physics at the UAB, and K. M. and S. P. thank the Department of Physics and Astronomy at SFSU for the hospitality. The work of D. B. was supported by the Gottfried Wilhelm Leibniz Programme of the Deutsche Forschungsgemeinschaft (DFG) and the Alexander von Humboldt Foundation. M. G. is supported in part by the U.S. Department of Energy under Contract No. DE-FG02-92ER40711, and J. O. is supported by the U.S. Department of Energy under Contract No. DE-FG02-95ER40896. S. P. is supported by Grants No. CICYTFEDER-FPA2011-25948 and No. 2014 SGR 1450, and the Spanish Consolider-Ingenio 2010 Program CPAN (Grant No. CSD2007-00042). K. M. is supported by a grant from the Natural Sciences and Engineering Research Council of Canada.

[1] M. Davier, A. Hoecker, B. Malaescu, C. Z. Yuan, and Z. Zhang, Update of the ALEPH non-strange spectral functions from hadronic $\tau$ decays, Eur. Phys. J. C **74**, 2803 (2014).

[2] D. R. Boito, O. Catà, M. Golterman, M. Jamin, K. Maltman, J. Osborne, and S. Peris, Duality violations in tau hadronic spectral moments, Nucl. Phys. B, Proc. Suppl. **218**, 104 (2011).

[3] R. Barate *et al.* (ALEPH Collaboration), Measurement of the spectral functions of axial-vector hadronic $\tau$ decays and determination of $\alpha_s(M_\tau^2)$, Eur. Phys. J. C **4**, 409 (1998); S. Schael *et al.* (ALEPH Collaboration), Branching ratios and spectral functions of tau decays: Final ALEPH measurements and physics implications, Phys. Rep. **421**, 191 (2005).

[4] M. Davier, S. Descotes-Genon, A. Höcker, B. Malaescu, and Z. Zhang, The determination of $\alpha_s$ from $\tau$ decays revisited, Eur. Phys. J. C **56**, 305 (2008).

[5] R. Shankar, Determination of the quark-gluon coupling constant, Phys. Rev. D **15**, 755 (1977); R. G. Moorhouse, M. R. Pennington, and G. G. Ross, Nucl. Phys. **B124**, 285 (1977); K. G. Chetyrkin and N. V. Krasnikov, Constraints on the behavior of the $e+e-$ hadron annihilation cross-section in asymptotically free theories and in theories with anomalous dimensions, Nucl. Phys. **B119**, 174 (1977); K. G. Chetyrkin, N. V. Krasnikov, and A. N. Tavkhelidze, Finite energy sum rules for the cross-section of $e+e-$ annihilation into hadrons in QCD, Phys. Lett. **76B**, 83 (1978); N. V. Krasnikov, A. A. Pivovarov, and N. N. Tavkhelidze, The use of finite energy sum rules for the description of the hadronic properties of QCD, Z. Phys. C **19**, 301 (1983); E. G. Floratos, S. Narison, and E. de Rafael, Spectral function sum rules in quantum chromodynamics: 1. Charged currents sector, Nucl. Phys. **B155**, 115 (1979); R. A. Bertlmann, G. Launer, and E. de Rafael, Gaussian sum rules in quantum chromodynamics and local duality, Nucl. Phys. **B250**, 61 (1985).

[6] E. Braaten, QCD Predictions for the Decay of the $\tau$ Lepton, Phys. Rev. Lett. **60**, 1606 (1988).

[7] E. Braaten, S. Narison, and A. Pich, QCD analysis of the $\tau$ hadronic width, Nucl. Phys. **B373**, 581 (1992).

[8] K. Ackerstaff *et al.* (OPAL Collaboration), Measurement of the strong coupling constant $\alpha_s$ and the vector and axial-vector spectral functions in hadronic $\tau$ decays, Eur. Phys. J. C **7**, 571 (1999).

[9] F. Le Diberder and A. Pich, Testing QCD with $\tau$ decays, Phys. Lett. B **289**, 165 (1992).

[10] K. Maltman and T. Yavin, $\alpha_s(M_Z^2)$ from hadronic $\tau$ decays, Phys. Rev. D **78**, 094020 (2008).

[11] O. Catà, M. Golterman, and S. Peris, Possible duality violations in $\tau$ decay and their impact on the determination of $\alpha_s$, Phys. Rev. D **79**, 053002 (2009).

[12] D. Boito, O. Catà, M. Golterman, M. Jamin, K. Maltman, J. Osborne, and S. Peris, A new determination of $\alpha_s$ from hadronic $\tau$ decays, Phys. Rev. D **84**, 113006 (2011).

[13] D. Boito, M. Golterman, M. Jamin, A. Mahdavi, K. Maltman, J. Osborne, and S. Peris, An updated determination of $\alpha_s$ from $\tau$ decays, Phys. Rev. D **85**, 093015 (2012).

[14] P. A. Baikov, K. G. Chetyrkin, and J. H. Kühn, Order $\alpha_s^4$ QCD Corrections to $Z$ and $\tau$ Decays, Phys. Rev. Lett. **101**, 012002 (2008).

[15] M. Beneke and M. Jamin, $\alpha_s$ and the $\tau$ hadronic width: Fixed-order, contour-improved and higher-order perturbation theory, J. High Energy Phys. 09 (2008) 044.

[16] S. Menke, On the determination of $\alpha_s$ from hadronic $\tau$ decays with contour-improved, fixed order and renormalon-chain perturbation theory, arXiv:0904.1796.

[17] I. Caprini and J. Fischer, $\alpha_s$ from $\tau$ decays: Contour-improved versus fixed-order summation in a new QCD perturbation expansion, Eur. Phys. J. C **64**, 35 (2009).

[18] S. Descotes-Genon and B. Malaescu, A note on renormalon models for the determination of alpha$_s(M_\tau)$, arXiv: 1002.2968.

[19] G. Abbas, B. Ananthanarayan, I. Caprini, and J. Fischer, Perturbative expansion of the QCD Adler function improved by renormalization-group summation and analytic continuation in the Borel plane, Phys. Rev. D **87**, 014008 (2013); I. Caprini, Strong coupling from the $\tau$ hadronic width by non-power QCD perturbation theory, Mod. Phys. Lett. A **28**, 1360003 (2013); G. Abbas, B. Ananthanarayan, and I. Caprini, Determination of the strong coupling from hadronic $\tau$ decays using renormalization group summed perturbation theory, Mod. Phys. Lett. A **28**, 1360004 (2013).

[20] A. A. Pivovarov, Renormalization group analysis of the $\tau$-lepton decay within QCD, Z. Phys. C **53**, 461 (1992); Yad. Fiz. **54**, 1114 (1991) [Sov. J. Nucl. Phys. **54**, 676 (1991)]; F. Le Diberder and A. Pich, The perturbative QCD prediction to $R_\tau$ revisited, Phys. Lett. B **286**, 147 (1992).

[21] M. Jamin, Contour-improved versus fixed-order perturbation theory in hadronic $\tau$ decays, J. High Energy Phys. 09 (2005) 058.

[22] A. Mahdavi, H. Hoekstra, A. Babul, J. Sievers, S. T. Myers, and J. P. Henry, Joint analysis of cluster observations: 1. Mass profile of Abell 478 from combined x-ray, Sunyaev-Z'eldovich, and weak lensing data, Astrophys. J. **664**, 162 (2007).

[23] S. Weinberg, Precise Relations between the Spectra of Vector and Axial Vector Mesons, Phys. Rev. Lett. **18**, 507 (1967).

[24] T. Das, G. S. Guralnik, V. S. Mathur, F. E. Low, and J. E. Young, Electromagnetic Mass Difference of Pions, Phys. Rev. Lett. **18**, 759 (1967).

[25] Y.-S. Tsai, Phys. Rev. D **4**, 2821 (1971).

[26] E. C. Poggio, H. R. Quinn, and S. Weinberg, Smearing the quark model, Phys. Rev. D **13**, 1958 (1976).

[27] O. Catà, M. Golterman, and S. Peris, Unraveling duality violations in hadronic $\tau$ decays, Phys. Rev. D **77**, 093006 (2008).

[28] O. Catà, M. Golterman, and S. Peris, Duality violations and spectral sum rules, J. High Energy Phys. 08 (2005) 076.

[29] B. Blok, M. A. Shifman, and D. X. Zhang, An illustrative example of how quark-hadron duality might work, Phys. Rev. D **57**, 2691 (1998); **59**, 019901(E) (1998); I. I. Y. Bigi, M. A. Shifman, N. Uraltsev, and A. I. Vainshtein, Heavy flavor decays, OPE and duality in two-dimensional 't Hooft model, Phys. Rev. D **59**, 054011 (1999); *At the Frontier of Particle Physics: Handbook of QCD*, Vol. 3, edited by (World Scientific, Singapore, 2001), p. 1447; M. Golterman, S. Peris, B. Phily, and E. de Rafael, Testing an approximation to large $N_c$ QCD with a toy model, J. High Energy Phys. 01 (2002) 024.

[30] M. Jamin, What two models may teach us about duality violations in QCD, J. High Energy Phys. 09 (2011) 141.

[31] M. Beneke, D. Boito, and M. Jamin, Perturbative expansion of $\tau$ hadronic spectral function moments and $\alpha_s$ extractions, J. High Energy Phys. 01 (2013) 125.
[32] K. Maltman, Constraints on hadronic spectral functions from continuous families of finite energy sum rules, Phys. Lett. B **440**, 367 (1998).
[33] C. A. Dominguez and K. Schilcher, Chiral sum rules and duality in QCD, Phys. Lett. B **448**, 93 (1999).
[34] See http://aleph.web.lal.in2p3.fr/tau/specfun13.html.
[35] For the results of this fit, see http://www.slac.stanford.edu/xorg/hfag/tau/hfag-data/tau/2009/TauFit_Mar2011/BB_PiKUniv/BB_PiKUniv_summary0.pdf.
[36] I. S. Towner and J. C. Hardy, Rep. Prog. Phys. **73**, 046301 (2010).
[37] J. Erler, Rev. Mex. Fis. **50**, 200 (2004).
[38] J. Beringer *et al.* (Particle Data Group), Phys. Rev. D **86**, 010001 (2012) and 2013 partial update for the 2014 edition; see http://pdg.lbl.gov.
[39] K. G. Chetyrkin, B. A. Kniehl, and M. Steinhauser, Phys. Rev. Lett. **79**, 2184 (1997).
[40] M. Jamin, Flavor symmetry breaking of the quark condensate and chiral corrections to the Gell-Mann-Oakes-Renner relation, Phys. Lett. B **538**, 71 (2002).
[41] C. Davies, K. Hornbostel, I. Kendall, G. Lepage, C. McNeile, J. Shigemitsu, and H. Trottier, Phys. Rev. D **78**, 114507 (2008).
[42] K. Maltman, D. Leinweber, P. Moran, and A. Sternbeck, Phys. Rev. D **78**, 114504 (2008).
[43] B. Chakraborty, C. T. H. Davies, G. C. Donald, R. J. Dowdall, J. Koponen, G. P. Lepage, and T. Teubner (HPQCD Collaboration), Phys. Rev. D **89**, 114501, (2014); C. McNeile, C. T. H. Davies, E. Follana, K. Hornbostel, and G. P. Lepage, Phys. Rev. D **82**, 034512 (2010).
[44] A. Sternbeck *et al.*, *Proc. Sci.*, LATTICE2007 (2007) 256 [arXiv:0710.2965]; LATTICE2009 (2009) 210 [arXiv:1003.1585]; A. Sternbeck, K. Maltman, M. Müller-Preussker, and L. von Smekal, *Proc. Sci.*, LATTICE2012 (2012) 243 [arXiv:1212.2039].
[45] B. Blossier, Ph. Boucaud, M. Brinet, F. De Soto, V. Morenas, O. Pène, K. Petrov, and J. Rodríguez-Quintero, Phys. Rev. D **89**, 014507 (2014); Phys. Rev. Lett. **108**, 262002 (2012).
[46] S. Aoki *et al.*, J. High Energy Phys. 10 (2009) 053.
[47] M. Baak, J. Cúth, J. Haller, A. Hoecker, R. Kogler, K. Mönig, M. Schott, and J. Stelzer (Gfitter Group Collaboration), The global electroweak fit at NNLO and prospects for the LHC and ILC, Eur. Phys. J. C **74**, 3046 (2014).
[48] J.-L. Kneur and A. Neveu, Phys. Rev. D **88**, 074025 (2013).
[49] A. Bazavov, N. Brambilla, X. Garcia i Tormo, P. Petreczky, J. Soto, and A. Vairo, Determination of $\alpha_s$ from the QCD static energy: An update, Phys. Rev. D **90**, 074038 (2014).
[50] E. Shintani, S. Aoki, H. Fukaya, S. Hashimoto, T. Kaneko, T. Onogi, and N. Yamada, Phys. Rev. D **82**, 074505 (2010); **89**, 099903(E) (2014).
[51] For an extensive list and discussion of recent determinations from DIS, jets and shape observables, see Sec. 1.2 of S. Moch, S. Weinzierl, S. Alekhin, J. Blumlein, L. de la Cruz, S. Dittmaier, M. Dowling, J. Erler *et al.*, High precision fundamental constants at the TeV scale, arXiv:1405.4781.
[52] I. Caprini, M. Golterman, and S. Peris, Functional-analysis based tool for testing quark-hadron duality, Phys. Rev. D **90**, 033008 (2014).